NTNU

Norwegian University of
Science and Technology

Rock Properties in Synthetic- and Natural Clay Materials

An Experimental Study on Shale Barrier Materials

Ivar Wathne Oftedal

Master of Science in Petroleum Geoscience and Engineering
Submission date: June 2018
Supervisor: Erling Fjær, IGP
Co-supervisor: Mohammad Hossain Bhuyian, SINTEF

Norwegian University of Science and Technology
Department of Geoscience and Petroleum

Acknowledgements

This report marks the end of my academic life as a student - a time that has presented me with many opportunities and wonderful experiences. There are many people I want to thank that have been important both in the writing of this thesis and during the time I have attended the University. The most significant of you are mentioned here.

First and foremost I would like to extend my gratitude to my supervisor Erling Fjær and co-supervisor Hossain Bhuyian at SINTEF Petroleum for accepting my request to write my Master's thesis as a part of the shale barrier project ongoing at SINTEF Petroleum. This report would not have been the same without your assistance and support.

To my fellow students at both the University of Stavanger and the Norwegian University of Science and Technology: I am sincerely grateful for the friendships we have made during the last five years. Hopefully our relationships can continue as we now enter our professional lives in the industry.

Lastly, I send my gratitude to my supportive family. I have taken a few turns during the last years - thank you for supporting me through them. To my nephew and niece, you have given me much motivation to complete my thesis in the best possible way - thank you.

Ivar Wathne Oftedal
Trondheim, June 2018

Summary

Since the late 1960's, thousands of wells have been drilled on the Norwegian Continental Shelf (NCS) - following the discovery of large hydrocarbon reserves on what eventually became Norwegian territory in the North Sea. Every drilled well has had its own purpose - exploration, production and/or injection. Independent of the purpose, every well has to undergo a series of mechanical operations in order to ensure that the hole will withstand the pressures in the underlying formations when the well reaches the end of its life and is plugged and abandoned.

For a number of years, plugging a well meant that the operator had to mill out large sections of casing in order to set cross-sectional cement plugs - an operation that is time-consuming and challenging because of the handling of the steel swarf from the milling process that must be circulated back to the surface and treated thereafter. In later years, as more focus has been shifted towards an effective plug and abandonment (P&A) approach, the cost of plugging operations have decreased substantially.

One method of special interest, that is the foundation of this thesis, is the application of mobile/ductile/plastic formations creating natural barriers in the annulus - primarily between the production casing and the formation. A naturally occuring rock with the properties to do so is to many known as shale. Shale is a broad term, but certain shale types have proven excellent in creating an impermeable and self-healing seal - a property that is not achievable in hardened cement.

A major part of this project has consisted of data acquisition from laboratory tests on different compositions of fine grained quartz (silt), kaolinite and smectite and also two naturally occurring shales - Pierre and Sele equivalent shale. These tests were performed in the Formation Physics laboratory of SINTEF Trondheim.

Given that kaolinite and smectite are two clay minerals with different properties, it was expected that a trend with regards to different ratios between sand, kaolinite and smectite and the transient permeability would be observed. This turned out correct as the permeability decreased with the increasing clay ratio in the samples. Especially notable

is the difference between kaolinite- and smectite samples, with a permeability at least one order of magnitude lower in the smectite samples (down to 5 nD).

The tests on the Pierre- and Sele shales were performed with some suspense as to how the samples would behave. The explanation is that the samples did not come in normal "core-geometries", but were crushed and mixed with brine before exposed to axial load. It turned out that as the samples were allowed to compact under axial loads in excess of 10 MPa, the behaviour during the tests approached that which one would expect from a "normal" shale sample regarding the tightness of the material.

Acoustic properties, porosity measurements and strain measurements have also been acquired, contributing to the acquisition of data in the rock samples that were tested.

Sammendrag

Siden slutten av 1960-tallet har tusenvis av brønner blitt boret på Norsk kontinentalsokkel (NKS) etter at man fant store hydrokarbonreserver på det som til slutt ble norsk territorium i Nordsjøen. Hver brønn har blitt boret med sitt eget formål - leting, produksjon og/eller injeksjon. Uavhengig av brønnens formål har alle brønner en fellesnevner - de må gjennom en rekke operasjoner for å sikre at hullet er i stand til å holde igjen på undergrunnstrykket når brønnen er ved slutten av sitt liv og skal forlates.

I mange år var plugging av en brønn ensbetydende med å frese ut lange seksjoner med foringsrør og deretter sette tverrsnittlige sementplugger i de samme intervallene - en prosedyre som er tidkrevende og utfordrene på grunn av nødvendig håndtering av stålspon som blir sirkulert opp til overflaten. I nyere tid, etterhvert som mer fokus har blitt rettet mot effektive pluggeoperasjoner, har kostnadene forbundet med brønnplugging sunket betraktelig.

Èn metode som er spesielt interessant i så henseende, som utgjør grunnlaget for denne rapporten, er bruken av duktile/plastiske formasjoner for å danne naturlige barrierer i ringrommet mellom produksjonsforingsrør og formasjonsbergart. En vanlig type bergart som i mange tilfeller er i stand til å gjennomgå deformasjoner uten å kollapse er skifer. Skifer er et vidt begrep, men enkelte skifertyper har vist seg å være utmerkede materialer for permanent plugging fordi de er lavpermeable og i stand til å "reparere" seg selv ved brudd. Dette er en egenskap man ikke ser i sprø sement.

En stor del av grunnlaget til denne rapporten har vært å innhente data fra transiente permeabilitets-tester på ulike sammensetninger av finkornet kvarts og leiremineraler (kaolinitt og smektitt). Disse testene har pågått på laboratoriet for formasjonsfysikk til SINTEF Trondheim.

På grunn av at kaolinitt og smektitt er leiremineraler med forskjellige egenskaper var det forventet å observere en trend i forhold til hvordan forskjellige blandingsforhold mellom kvarts/kaolinitt/smektitt ville påvirke transient permeabilitet. Dette viste seg å stemme ettersom en klar indikasjon på lavere permeabilitet ettersom leireinnholdet økte. Spe-

sielt merkbart er forskjellen mellom kaolinitt- og smektittprøver, med en permeabilitet i smektittprøvene på minst èn størrelsesorden mindre (5 nD).

Testene på Pierreskifer og Sele-ekvivalent ble gjennomført med noe spenning i forhold til hvordan prøvene ville oppføre seg i løpet av testen. Grunnen er at disse to prøvene ikke kom som ferdige kjerneprøver, men ble fremskaffet ved å knuse skifermateriale for deretter å legge det knuste materialet i en tykkvegget sylinder, blandet med saltvann, og la de bli kompaktert av en aksiell last. Etterhvert som aksiell last økte begynte prøvene å utvise mer og mer "skiferlignende" oppførsel.

I tillegg til permeabilitetsmålinger ble det også gjort målinger av porøsitet, p-bølge-hastighet og strekk i alle prøvene som ble testet - noe som bidro til å fremskaffe mer data om materialet som ble testet.

Contents

List of Figures

List of Tables

1 Objectives of Project

The objective of this project has been to study transient permeability and ultrasonic wave behaviour in consolidated mixtures of quartz and clay minerals and in crushed shale material under different compaction loads. The aim is to obtain more information about the potential these materials have in shale-barriers, and how they might be identified on an acoustic based wireline log.

2 Introduction

2.1 Background

New or old, good integrity or bad integrity - every well that has been drilled on the Norwegian Continental Shelf(NCS) has led a unique life. For millions of years, the source rocks, reservoirs and overburden sections on the NCS were free to consolidate, deform and store by themselves. Suddenly, in the 1960's, humans started interfering as it was discovered that the economic potential hidden in the NCS underground was beyond comprehension.

As a new hole was (and is still being) made, a new P&A job was (and is) created for the future. On a global scale, it has been estimated that roughly 75% of all drilled formations are shales (Lal, 1999). In Norwegian overburden sections, shale rocks are abundant, giving us the opportunity to exploit the beneficial properties in many shales with regards to obtaining an "impermeable" seal after abandoning a well.

When a well is drilled, alterations are made to the stress state in and around the borehole. What was once solid rock formation becomes a hole in the ground with a new stress distribution around it. At the end of the life of the well, the operator needs to re-plug the hole. Ideally, the rock should be returned to its initial state (restoring the cap rock), a task practically impossible. However, one still has good opportunities to create a seal in the hole that will act as a plug against the pressure from below.

For a very long time, the most common method to establish such a barrier was to enter the hole with large milling tools with the aim to remove long sections of the casing to accommodate for a cross-sectional cement plug inside the hole. If successful, the requirements from NORSOK D-010 have been met and after good pressure testing of the plug, one has a plug with good integrity. The NORSOK D-010 document is a part of the NORSOK (NORsk SOkkels Konkurranseposisjon) initiative and is a document created by the Norwegian petroleum industry. The document contains requirements and guidelines regarding the safe management and maintenance of well integrity during all stages in the

life of a well - drilling, production/injection and P&A. In Figure 2.1, the concept of a cross sectional plug is displayed.

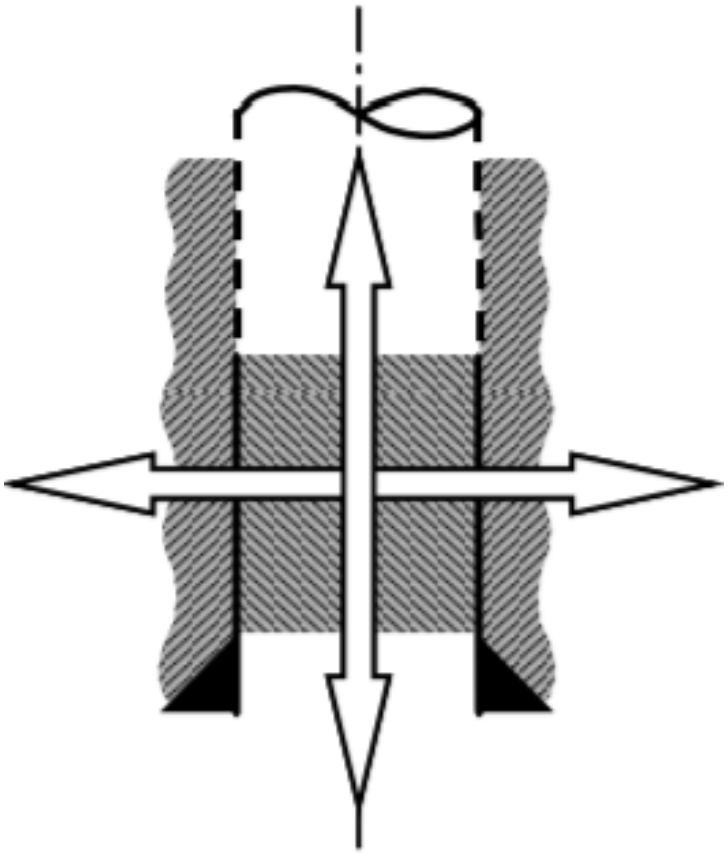

Figure 2.1: *A cross sectional plug (NORSOK D-010, 2013 p. 96)*

Cement has traditionally been the dominating plug material material. However, it is still not an ideal material for plugging applications as it deteriorates over time when exposed to acids and altered downhole conditions. Plus, being a brittle material makes the integrity of cement vulnerable to fractures. More on the comparison between shale and cement follows in Chapter 4.

Note that set cement in everyday language is better known as concrete. In the oil industry however, the reigning term is cement - even when hardened. Therefore, cement will be used consequently throughout this report.

In later years, especially after entering the new millennium, several wells on the NCS have been, using wireline logging tools, proven to have annular seals in the production casing interval above the top of cement (TOC). As it was ruled out that this could be explained

by settling baryte in the annular fluid, it was concluded that the sealing material was reservoir overburden formation that had deformed and impinged onto the production casing outer wall. The ductile properties of many shales causing significant down-time in drilling operations were now presented as something that could be applied in a P&A setting.

According to the guidelines in NORSOK D-010, a plug established in a P&A job has to satisfy the following criteria:
a) Provide long term integrity (eternal perspective);
b) Impermeable;
c) Non-shrinking;
d) Able to withstand mechanical loads/impact;
e) Resistant to chemicals/substances (H_2S, CO_2 and hydrocarbons);
f) Ensure bonding to steel;
g) Not harmful to the steel tubulars integrity.
(NORSOK D-010, 2013, p. 96). In other words, the requirements do not refer to a specific barrier material, but rather the properties a barrier must possess. Many shale types meet these requirements, thus constituting a perfect barrier material where it is applicable.

Despite the fact that shale deformation mechanisms are far from fully understood, many annular shale barriers have already been tested and verified as part of primary/secondary barriers on the NCS. At the moment, it seems that the biggest challenge regarding shale barriers is how to actively induce and/or anticipate a plastic response from the formation - making it impinge onto the outer casing wall. One way considered is to induce chemical reactions by exposing the formation to proper fluids. Another method is to create a hydraulic underbalance in the annulus, thus provoking a borehole wall deformation inwards - more about this in Chapter 4.

This report will, in addition to elaborating on the principle of shale annular barriers, present results from experimental laboratory tests conducted on powdered quartz/clay samples and crushed natural material (Pierre shale and Sele equivalent). These tests are performed with the aim to provide SINTEF with a data set that is reliable and where the approach in the laboratory and evaluation of data are well documented.

2.2 P&A - The Bigger Picture

For the average Norwegian citizen, detailed knowledge of the application of various materials in a P&A setting may not be very intriguing. However, the potential in technology that makes the plugging activity more efficient (ie. cheaper), should be of interest to everyone. In Norway, the state gets 78% of all production-related income. The same percentage of plugging costs will however also be covered by the state - which in practicality means the Norwegian tax payer. With several estimates indicating that the total bill for decommissioning activities on the NCS will amount to over 2,000 billion NOK, it is safe to say that even the slightest improvement in plugging efficiency has the potential of saving the state for considerable sums of money - thus accommodating for a better use of those funds, for example the bettering of the infra-structure and the educational system.

In addition to the use of plastic shale formations, several methods concerning permanent P&A are in development. A lot has also been achieved already on that front. Most notable is perhaps the introduction of perforate-wash-cement (PWC) technology. The essence of this method is to use explosive charges to blow holes in the casing. Subsequently, the casing inside and outside are washed thoroughly with a high powered jetting tool before cement is eventually pumped down in the perforation interval - leaving cement both on the inside and outside of the casing. By using this method, the operator does not need to be concerned with the mechanical removal of casing string by milling. The PWC-method has already reduced the average plugging time on the NCS by several days and continues to be the method of choice unless a better alternative is available.

In the future, more focus on advancement in P&A is important to ensure a continued progression in the technology. PWC-technology is well established, other methods like the use of plastic shale formations, thermite technology etc. are also continuously being considered and potentially improved. In the long run, the ultimate goal for operators on the NCS is to be able to set and verify good plugs without the need for a derrick - in which case a jack-up rig has to be hired and placed over the well when the rig does not have the derrick itself. A rig-less solution will most likely be available by wireline.

Alternatives are currently under development, with the use of shale being one of them.

2.3 Report Structure

This report is constructed so that the reader may obtain a clear understanding of shale and what type of material it is before embarking on experimental methodology and results. Initially, from a mechanical point of view, we will visit some theory regarding stress development in a wellbore geometry using basic principles. Further, a comparison of flow potential in a typical Portland cement and shale cement will be presented. In addition to geomechanical principles, one cannot avoid to talk about chemically induced instability in shale as this is something that has caused problems for drilling operations worldwide since the beginning of drilling wells in clay-rich rock formations.

After the initial chapters, more detail on the current project follows. Laboratory methodology and results from the tests will be presented and discussed before concluding remarks with recommendations for possible future studies will be given.

3 Materials in testing

In Chapter 2, the permanent plug requirements from the NORSOK D-010 document were rendered. Given that the current project has its base in shale studies, it is natural to clarify why a rock with high clay content might satisfy the requirements that are specified in NORSOK D-010.

In the laboratory work, quartz and two clay minerals have been tested under same conditions. The synthetic clay minerals were from the montmorillonite and kaolinite group - two types of clay minerals with notably different properties.

In addition, two tests with naturally occurring material has been performed. These two materials were Pierre shale and a Sele shale equivalent.

3.1 Quartz

In all the tests with synthetic materials, Ottawa sand with grain size distribution between 355μm and 230μm was applied in the quartz/clay mix. As the name implies, it is harvested from deposits in Ottawa, Illinois. It is ideal in the way that is consists of more or less 100% of well rounded grains. Naturally, the amount of quartz in each test sample makes a big impact on the mechanical properties of the sample. More detail on specific impact of quartz content will be presented in Chapter 6. However it should not be surprising that due to the considerably larger quartz grains compared to the clay plus a higher bulk modulus that resists compression, the quartz grains relatively quickly constitute a load-bearing matrix - especially in samples where the clay content is low.

3.2 Powdered clay

Shales are sedimentary rocks with a mineralogy dominated by clay where the load bearing matrix is constituted by clay minerals, meaning that the clay content is 40% or higher (Fjær et al. 2008). Figure 3.1 from Swan et al. (1989) displaying a scanning electron

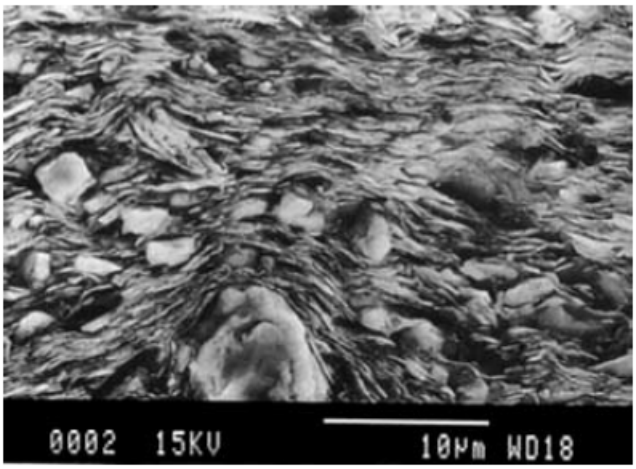

Figure 3.1: *A Scanning Electron Image of Kimmeridge shale (Swan et al., 1989 p. 137)*

image of a Kimmeridge clay shows how the clay particles are arranged on the molecular level.

The structural features of clay minerals are very distinctive, albeit with different elements constituting the structure. Common for clay minerals is the sheet-like geometry where the sheets of crystal structures are arranged in planes parallel to the bedding plane. This is easily observed if one attempts to break a piece of shale. The fracture surface will be slick and smooth if the fracture happens along the bedding planes (slickenslides), but with an irregular surface if fractured perpendicular to the bedding planes. Table 1 with values from Juma (1998), rendered by Asef and Farrokhrouz (2013) is included to show more of the features in normal clay minerals.

An important factor contributing to the normally low permeability is the small particle size leading to very small pore throats in a consolidated shale. For these rock types, permeability in the nano-Darcy (nD) range is typically found. This also holds true for many shales with relatively high porosity - due to small particle size.

Now, what is it that in many cases makes shale problematic to drill through? In the subject of shale instability and swelling shale, the negative charge of clay platelets are important. Figure 3.2 is a simple sketch of the phenomenon. As the platelet surfaces are negatively charged, cations and/or dipolar water molecules are attracted to the surface. Thus, when such particles are present, a potentially volume-increasing process is initiated which can lead to pore pressure build-up and significant altering of the borehole geometry

Properties of three common silicate clay minerals

Property	**Montmorillonite**	**Illite**	**Kaolinite**
Size (μm)	0.01-1.0	0.02-2.0	0.5-5.0
Shape	Flake	Irregular flakes	Hexagonal crystals
External surface area (m^2/g)	70-120	70-100	10-30
Internal surface area (m^2/g)	550-650	-	-
Plasticity	High	Medium	Low
Cohesiveness	High	Medium	Low
Swelling capacity	High	Low to none	Low
Unit-layer charge	0.5-0.9	1.0-1.5	0
Interlayer spacing (nm)	1.0-2.0	1.0	0.7
Bonding type	Van der Waal's weak attractive force	Potassium ions	Hydrogens
Net negative charge ($cmol_c/kg$)	80-120	15-40	2-5

Table 1: *Three common silicate clay minerals (Juma, 1998)*

Figure 3.2: *Negative clay platelet attracting cations*

due to packoffs or even collapse of the wellbore.

Drilling instability is not within the scope of this report. However, the following summed up factors contributing to a destabilized shale are significant also when considering a specific shale for P&A-purposes:

1. Salinity of fluid in contact with formation relative to the pore fluid in the formation
    - We refer to this as water activity, $A_{w,mud}$, compared to the water activity of the shale pore water, $A_{w,shale}$, which is inversely proportional to the salinity of the fluid. Therefore, low salinity means high water activity - a low saline fluid will move towards a higher saline fluid (osmosis)
2. Electrostatic charge of clay surfaces

3. CEC - The ability of the shale to retain cations on the surface of the platelets.

    - This property depends on what type of cations are in use

From Asef and Farrokhrouz (2013), the following order of cation exchange is obtained:

$$Na^{+}<K^{+}<Mg^{2+}<Ca^{2+}<H^{+},$$

Meaning that a potassium ion will tend to swap position with a sodium ion already in place between the clay layers. If the size of the exchanging cations taking place is less than the prior, then a swelling-inhibitive process has occurred.

A brief consideration of the materials in the laboratory experiments follows.

3.2.1 Kaolinite

Kaolinite is arranged in a layered mineral structure with the chemical formula $Al_2Si_2O_5(OH)_4$. The composition and placement of atoms are more easily understood when considering the geometric structure of the platelets. Kaolinite consists of layers of silica tetrahedons (Si-atom surrounded by four O-atoms) and aluminium octahedrons (Al-atom surrounded by six hydroxyl (OH) groups).

Figure 3.3 displays the structure in normal kaolinite where all the above mentioned constituents can easily be observed. Covalent bonds between oxygen atoms make up tetrahedral sheets with hydroxyl groups in the aluminium octahedrons bond the sheets together. From Asef and Farrokhrouz (2013, p. 7): 'The H-bond force in Kaolinite is stronger than other clay minerals which leads to low cation adsorption and makes a hexagonal shape with 0.1-5 μm particle size'.

3.2.2 Montmorillonite

Montmorillonite is the other clay mineral group from which a synthetic, powdered clay has been used in the laboratory work.

The chemical formula is $(Na,CA)_{0.3}(Al,Mg)_2Si_4O_{10}(OH)_2\cdot nH_2O$ and it is useful in industry due to its high cation exchange capability and tendency to expand in water. More properties are seen in Table 1 - from where it is obvious that the montmorillonite group

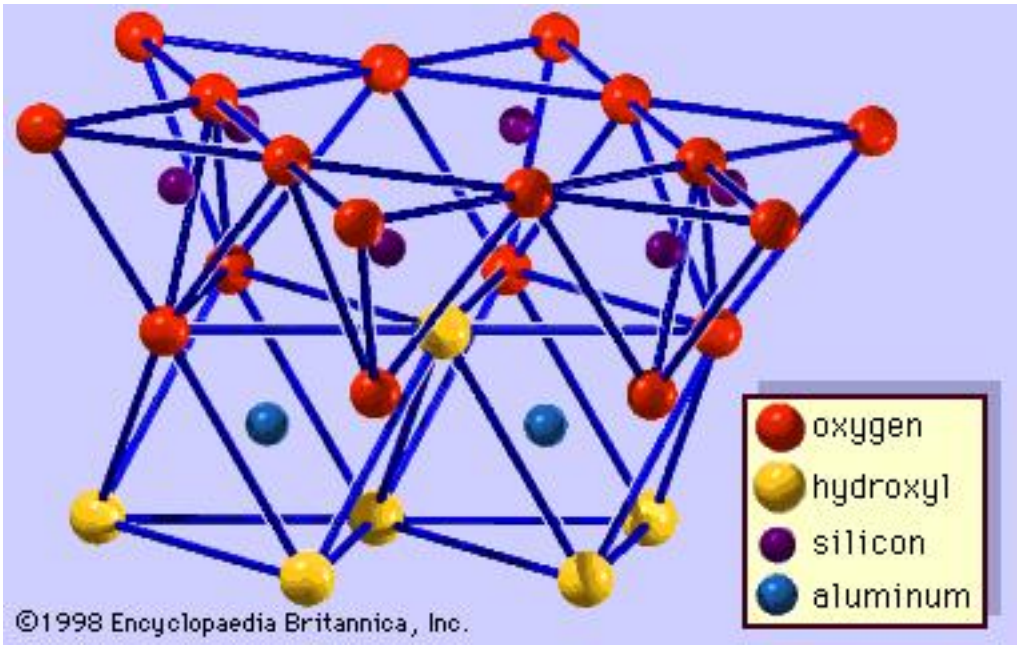

Figure 3.3: *Kaolinite sheet structure (Encyclopaedia Britannia)*

differs quite a lot from the kaolinite group. Given montmorillonite's larger surface area and net negative charge, it becomes apparent that such a mineral is very reactive with water.

According to Baptist and Land (1965), all clay minerals absorb water on their surfaces, but only in montmorillonite is water absorbed between inter-crystalline layers - making it more susceptible to expansion/swelling.

Note: In many cases, montmorillonite is referred to as smectite simply because montmorillonite is a member of the smectite group. Therefore, any mentioning of smectite in this report will be a reference to the montmorillonite mineral that is used in the tests - unless otherwise is specified.

3.3 Pierre shale

Pierre shale is a naturally occurring shale from a geologic formation east of the Rocky Mountains in the USA. In most Pierre shale, clay minerals make up the dominant bulk volume, although, according to Boerngen et al. (1980 p.12), other common minerals like quartz, feldspars, calcite or zeolites can be dominant in some samples. The Pierre shale

in the experiment had several minerals in the mix, the most abundant being quartz, illite and plagioclase. Normal Pierre shale from the field has a porosity of around 18-20%.

From the author's research, several experiments have already been performed by previous MSc-students writing for SINTEF, although with an aim that is more focused on the creep and consolidation behaviour of the material, and not so much permeability. Therefore it was decided to include a Pierre shale sample in the tests of this study as well.

3.4 Sele equivalent

The Sele equivalent shale has very characteristic features when it comes to composition and mechanical properties. Because the Sele material in the experiments was considerably more ductile than the Pierre shale, it could not be crushed in a mortar in the exact same way, but had to be broken into sufficiently small pieces, weighed and then put into the cylinder for compaction.

The quartz content is low compared to Pierre shale, with only 9.6%. 26.1% consists of kaolinite and 19.5% of the material is illite. It can be mentioned that the smectite content is 1.8% in the illite, compared to 4.5% in the Pierre shale.

4 Shale as a barrier

In this section, a few methods regarding how the operator might induce a shale annular barrier will be considered. Clear methods for obtaining annular formation barriers that have good integrity are not completely established in current practice, however there are several theoretical approaches that need further consideration. The aim of this chapter is to provide some insight into different possible methods.

Before presenting the methods, some theory regarding wellbore mechanics as well as other phenomena like thermal expansion/contraction will be discussed. This will aid in establishing a foundation to understand why a certain method might help to induce a response from the formation that may create an annular seal.

In this section, and throughout the remainder of the report, the concepts of compressive and tensile loads are important. Because compressive loads will play a "larger" role in the report than tensile loads, we define compressive loads as positive and tensile loads negative - for convenience.

4.1 Rock mechanics

In a borehole, the initial stress state is altered when the formation is penetrated by the drill bit. Many factors play a role when determining the stress state in the rock, for example inclination and the in-situ horizontal stresses. However, for simplicity, a classical approach is to view the borehole as a plate with a hole in the middle - as in Figure 4.1.

The stresses σ_h and σ_H denote the minimum and maximum horizontal stresses, respectively. In some cases, to simplify the problem, we assume $\sigma_h = \sigma_H$. Further simplification leads to the assumption of a vertical hole, leading to the following equations for axial stress σ_z, radial stress σ_r and tangential stress σ_θ (Miska & Mitchell, 2011):

$$\sigma_r = P_w \tag{4.1}$$

$$\sigma_\theta = 2\sigma_h - P_w \tag{4.2}$$

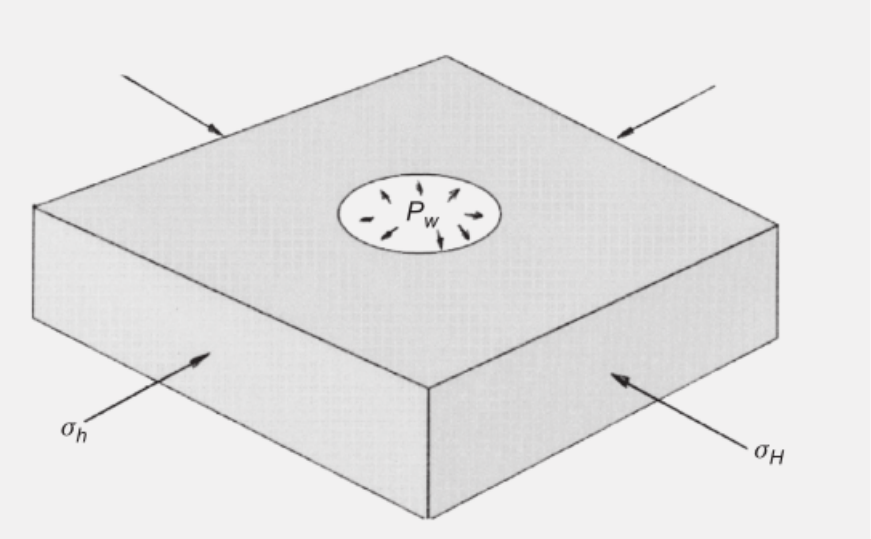

Figure 4.1: *Visualization of the borehole (Miska & Mitchell, 2011, p. 62)*

$$\sigma_z = constant \tag{4.3}$$

Where the three stresses act as displayed in Figure 4.2.

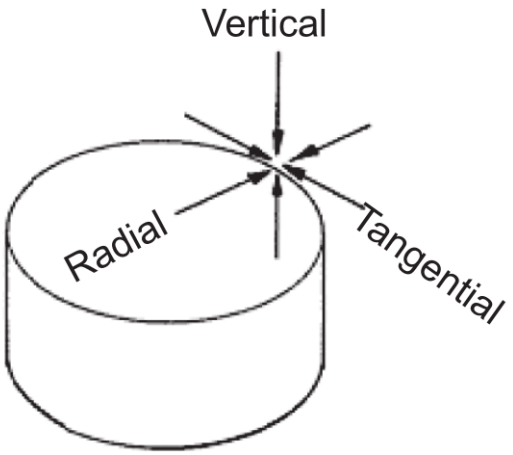

Figure 4.2: *Stresses acting on the borehole wall, vertical hole (Mitchell & Miska, 2011, p. 70)*

In the "classical" drilling approach, these are the basic stresses the drilling engineer needs to understand when planning how to keep the hole stable during the drilling operation.

The same stresses act in the borehole wall in the annulus outside of a production casing. Depending on whether there is good cement present, settled mud weight material or just fluid - the stress state in the formation is determined. In a case where plugging is imminent, naturally the operator needs to know what material/fluid is present in the

production casing annulus to know whether the formation can be "accessed" or not.

Trying to induce a mechanical response from the formation would have to be done by altering the pressure regime in the annulus in some way. For example, the response when going underbalanced in a well/annulus could be inflow of formation fluid (if permeable enough rock), or shear failure in the rock itself. The simplifying assumption of a vertical hole with $\sigma_h = \sigma_H$ is not realistic in many cases, but it is clear from the equations what happens when altering the borehole pressure. Further, many overburden intervals through shale layers on the NCS are nowhere near the inclination one can observe in certain reservoir sections. Therefore the vertical hole assumption with $\sigma_h = \sigma_H$ will be widely used in this discussion.

As the axial stress remains constant, the tangential compressive stress is seen to increase when borehole pressure is decreased, and vice versa. Meaning that there are in general two failure mechanisms that can be "induced" by the operator - collapse (shear failure) or fracturing (tensile failure), displayed in Figure 4.3:

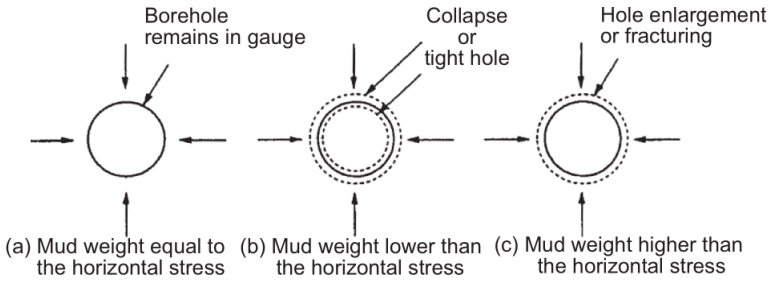

Figure 4.3: *Formation responses to pressure in borehole (Mitchell & Miska, 2011, p. 63)*

Naturally, it is challenging to predict exactly what type of response one will see from the formation if the annulus pressure is in some way altered. What is certain is that any type of material will exhibit some sort of deformational behaviour if exposed to sufficient stress over time. The behaviour of materials when exposed to stress is divided mainly into elastic and plastic regions, and we will take a short look into these in the following.

4.1.1 Elastic behaviour

Elasticity refers to the property of a material that makes it able to return to initial atomic plane configuration after undergoing stress causing a deformation. Naturally, this is not

the kind of behaviour that is desired in P&A applications as a sealing barrier must be permanent - making permanent deformation of the rock more suitable. Nevertheless, to understand both concepts, some theory on elasticity will be briefly discussed.

The elastic behaviour of a material is often displayed as a perfect linear relationship between applied stress (σ) and resulting strain (ϵ). The resulting strain describes either a change in length, L:

$$\epsilon = \frac{\Delta L}{L} \tag{4.4}$$

Or, we use a measure referred to as shear strain, γ, when shear stress is introduced to the sample (compressive axial force causing shear deformation):

$$\gamma = \frac{1}{2} tan(\psi) \tag{4.5}$$

Where the angle ψ is the change in angle between two directions in the material, causing the need for a two-dimensional view like in Figure 4.4 (Fjær et al., 2008), where τ denotes shear stress in the plane.

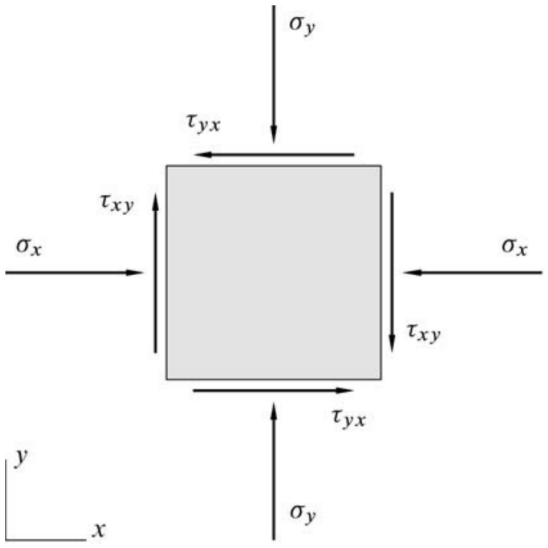

Figure 4.4: *2D-view of stress components (Fjær et al., 2008, p. 4)*

A simple example is a uniaxial/triaxial unconfined/confined test where a material specimen undergoes either tensile or compressive stress in the axial direction - either with or without confining pressure. In initial stages of the test, the planes in the material on the molecular level are redistributed with no bonds broken, allowing the specimen to return

to original shape and size when axial force is relieved. Depending on the ductility of the material, the degree of deformation it can undergo and still return to initial shape will vary. For example, steel exhibits more ductile behaviour than brittle cement.

For such purposes, $sigma = \frac{F_n}{A}$ describes the resulting stress from the force F. Note that F must be decomposed into parallel and normal component when calculating normal and shear stress on a plane, hence the subscript n for "normal". For shear stress on an area, the parallel force component is used, $\tau = \frac{F_p}{A}$.

Further, a linear relationship between stress and strain is described using Hooke's law:

$$\sigma = E\epsilon \tag{4.6}$$

Where E denotes the modulus of elasticity, or Young's modulus - representing the ability of the material to resist being elongated by an axial tensile force. We separate between what kind of elastic response is seen in a material during a loading/deloading phase as different materials exhibit different elastic responses. Figure 4.5 from Fjær et al. (2008) displays different loading/deloading paths: A linear elastic response, a non-linear perfectly elastic response and an elastic response with a hysteresis path - meaning that deloading path is different from that in the loading sequence. In Figure 4.5, the last

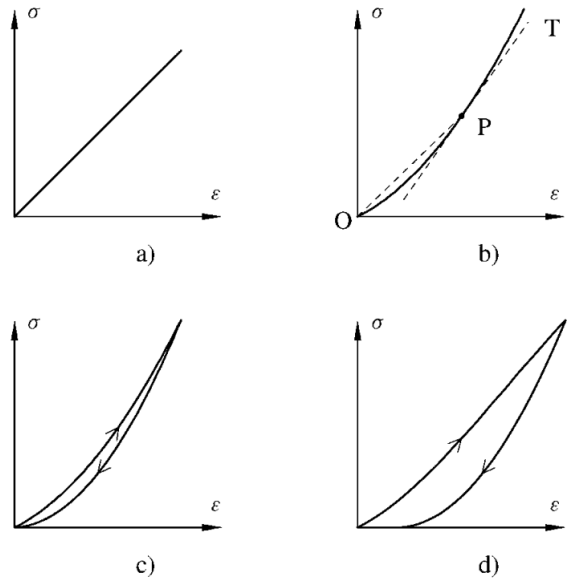

Figure 4.5: *Different elastic responses, plastic deformation in d) (Fjær et al., 2008, p. 42)*

example (d) is a case of resulting plastic (permanent) deformation, which brings us to the next section where plastic behaviour will be briefly discussed.

4.1.2 Plastic Behaviour

As already stated, a plastic response is ideally what the operator would try to induce from the formation in the annulus - if trying to create a formation barrier. Such a response would be especially beneficial if occurring directly after the production casing is set and cemented into place as that would mean further annular barriers above the TOC. However, the unpredictable behaviour of shale makes it a difficult task to predict whether a deformation will occur or not.

The transition between elastic and plastic region in a material occurs at what is called the yield point, σ_y. As soon as this stress level is exceeded, the material in question can no longer return to original atomic configuration because bonds in the atomic structure have been permanently broken. More specifically, atom planes have slipped along weak locations and irregularities in the structure - known as dislocations.

Figure 4.6 (Fjær et al. 2008) displays a typical curve where a specimen is loaded until failure occurs. The different regions on the curve are of course different depending on what material is being tested. The following explanations for each region are given by Fjær et al. (2008, p. 56):

Elastic region: The rock deforms elastically. If the stress is released, the specimen will return to its original state.

Yield point: The point beyond which permanent changes will occur. The sample will no longer return to its original state upon stress relief.

Uniaxial compressive strength: The peak stress.

Ductile region: A region in which the sample undergoes permanent deformation without loosing the ability to support load.

Brittle region: A region in which the specimen's ability to withstand stress decreases rapidly as deformation is increased.

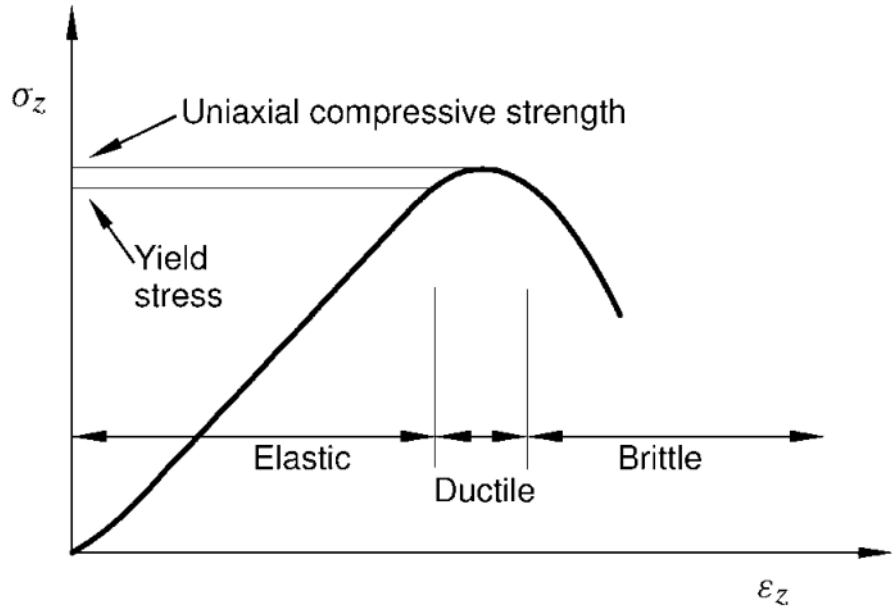

Figure 4.6: *General deformation path in a uniaxial compression test (Fjær et al., 2008, p. 56)*

The different phases of deformation on the curve in Figure 4.6 can be related to different states in the sample undergoing the loading. It is important to note the generality of this curve - one cannot directly compare the behaviors in two different materials, the curve in the figure only displays a general behaviour.

Tests resulting in such stress-strain plots are usually performed by exposing the test specimen to axial and confining stresses - a triaxial test. After reaching a certain confining load, which is perpendicular to the axial direction, only the axial load is altered from then on. In such tests, there are normally two failure mechanisms observed, depending if the sample is in compression or tension. Briefly described earlier, shear stress is calculated from a force component parallel to the failure surface - while tensile stress is found using the normal component. Figure 4.7 from Fjær et al. (2008) displays the difference between the two failure mechanisms.

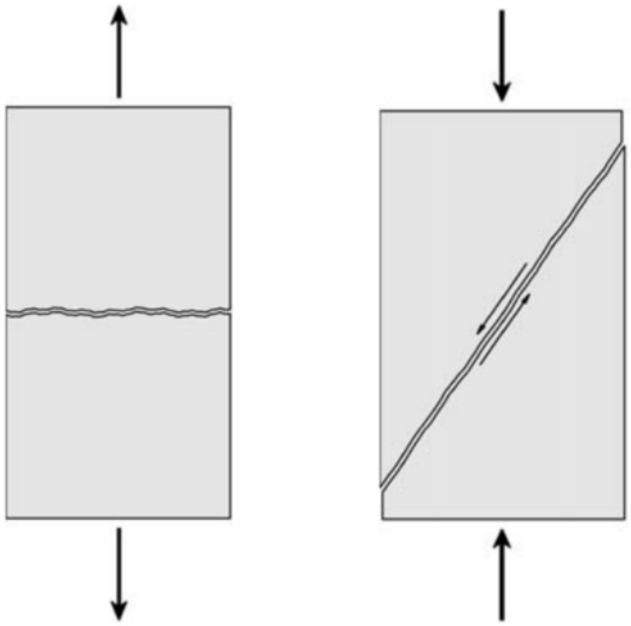

Figure 4.7: *Tensile (left) and shear (right) failure (Fjær et al., 2008, p. 60)*

4.2 Inducing a Formation response

In a typical overburden rock being penetrated by a drill bit, like a clay-rich shale on the NCS, the large overburden load compresses the rock, thus affecting the axial stress in the borehole wall. Further, the horizontal stress development largely depend on the conditions in the hole. If the annulus conditions can be stimulated to create a large underbalance, it is evident from equation 4.2 that radial stress decreases and tangential stress increases - meaning that effective stress on rock matrix becomes compressive and the rock comes closer to a failure state.

Depending on mineralogical composition, shale may act as a material with very beneficial ductile properties - meaning that upon failure it may have the ability to self-heal its cracks. This is a property not seen in brittle cement, making shale an obvious candidate material for long term barriers. This especially holds true when considering the low permeability found in many compacted shales.

4.2.1 Underbalance in annulus

If the stress acting upon the shale matrix is large enough, with sufficiently small strength in the matrix, the load might be enough to seal potential cracks in the rock, as is shown in Figure 4.8, taken from a presentation held by Tron Kristiansen from BP (now Aker BP), October 2015 at a P&A forum in Stavanger, Norway. In the figure, the term EDZ refers to Excavation Damage Zone - meaning a zone around the wellbore damaged during the drilling process. Depending on several conditions, the cracks may dilate or contract, the latter being desirable for plugging purposes.

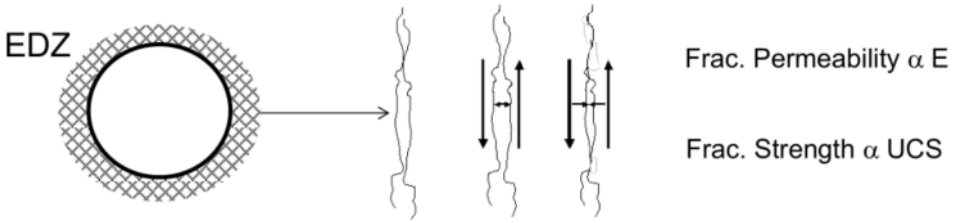

Figure 4.8: *Cracks either dilating or contracting (Tron Kristiansen, BP 2015)*

Pointed out in the figure are also relationships between permeability and Young's modulus and between fracture strength and uniaxial compressive strength (UCS). As E basically describes the stiffness of the rock, naturally low values correspond to a ductile material that gives in for a load, leading to lower permeability when crack diameter shrinks. Also for low UCS-values in the rock, the cracks will have a higher chance of "healing" themselves because the rock then has a lower threshold before deforming.

In his presentation from 2015, Kristiansen also presented a case from a drilling liner incident while drilling in a Paleocene interval in the North Sea. Figure 4.9 is taken from this presentation and displays the pressure development during drilling into a depleted reservoir section where pore pressure was considerably lower than in the well. There are five events circled in the figure. The events were these:

1. Initial pressure was 41 MPa
2. A sudden pressure drop lasting about 2 minutes happened when the depleted reservoir was hit, pressure decreased to 20 MPa
3. Low annulus pressure was sustained until ball was seated

4. Pressure increased while the pump rate needed in the annulus decreased

5. The pressure increased up to 39 MPa

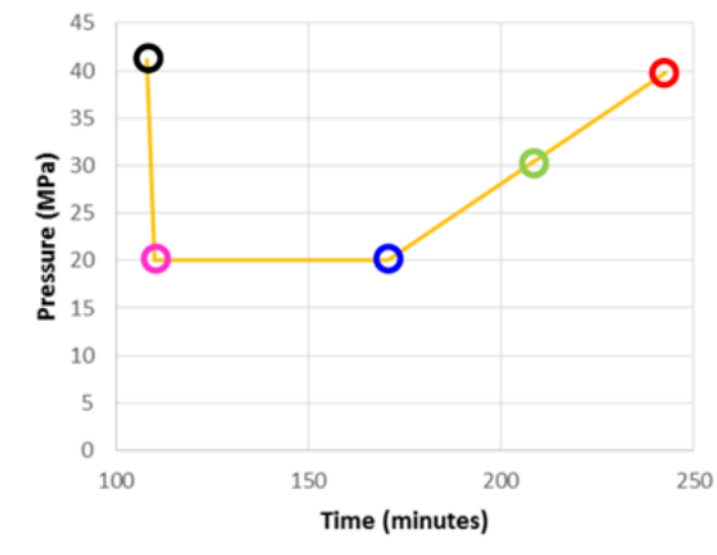

Figure 4.9: *Annulus pressure development after mud loss (Tron Kristiansen, BP 2015)*

Although drilling liner technology is an interesting subject, it will not be discussed further in this report.

The reason for the sudden pressure decrease between the two first points in Figure 4.9 was the large overbalance ($P_{well} >> P_{pore}$) in the hole causing the formation to fracture and the mud to flow into it (mud losses). Until the drop ball was seated inside the downhole tool, low pressure in the annulus was sustained. Further, the pressure again started to increase while the needed rate was lower (according to BP) - indicating a decrease in diameter of the hole. In other words, the formation responded to the underbalance situation and rapidly started to move radially inwards.

The question then becomes: Is it possible to achieve the same outcome in a controlled pressure cycle process where simple downhole mechanics are used to induce a deformation in the rock? The answer remains unclear and although it is not the essence of this report, it is worth noting that inducing underbalance in the annulus may allow the formation to deform inwards. Perhaps even more when combined with other mechanisms that will be mentioned later in this section.

In a case where a fluid column is present above the TOC in a production casing annulus,

trapped volumes between formation and casing wall is a possible explanation as to why not a higher number of natural occurring annular shale barriers have been observed on the NCS. The principle is quite simple; Assume that there is indeed an initial underbalance situation in the annulus, allowing the formation to deform inwards. Also assume that there is no possibility for bleeding off the annulus pressure. If then the formation was to move in on the casing, the annulus volume would decrease - leading to a pressure increase. Unless this pressure is allowed to be bled off either on wellhead or through the formation itself, the formation would possibly have a sufficiently large resistance against fully impinging onto the outer casing wall. More about this in section 4.4.

4.2.2 Chemically induced formation response

When considering shale formation in a well engineering context, the first thing that may come to mind is the classical problem related to shale instability while drilling - due to an unwanted interaction between the base fluid in the drilling mud and the rock. For a long time this was a large time-consumer in the industry. After the introduction of oil-based mud (OBM) systems, these problems have to a large extent been dealt with. However, common classical shale issues present an alternative to how one might induce a formation response in a P&A-setting, therefore it is important that chemically induced instability in shale is also considered.

In Chapter 3, some basic theory regarding the composition of common clay minerals was presented. It was said that certain clay minerals are more susceptible to causing a swelling related problem when exposed to water than other minerals. Moreover it is well established that a drilling engineer can expect to encounter considerably more shale-related drilling problems in some specific shales. Thus, depending on what composition the shale surrounding a production casing annulus has, the operator might be able to apply this to own benefit by exposing the formation to some reactive fluid - the opposite of what one would do when initially drilling the well.

The question that remains is whether or not a chemically induced deformation will be sufficient to close of an entire annulus - and if that happens, will the seal remain permanent?

There is no definite answer to that question.

In 2016, the author was involved in a project for ConocoPhillips Norway where the goal was to map wells that had been plugged using shale barriers on the Ekofisk field during 2015 and 2016 and from old reports find out what type of fluid had been used during drilling and as fluid above top of cement. The results from that project indicated that if one wants to predict a formation seal, chemical mechanisms were not enough to conclude whether a barrier would be in place or not.

On the NCS, there are several sites with an overburden formation that could present operators with potential formation seals. On the Ekofisk field, ConocoPhillips Norway (COPNO) have encountered several wells where wireline logs run prior to plugging have shown that long intervals in the annulus have been completely filled with deformed formation rock. Some information about two wells has been obtained, one of which had a clear indication of a formation seal outside the production casing. Whether this was due to chemical reactions or not is unclear as other factors are also at play. These real cases are presented in section 4.4.

In addition to the above mentioned theory, one should also consider the possibility of temperature induced deformation in clay-rich shale.

4.2.3 Thermal response in shale

It is quite intuitive that an alteration in temperature causes some volumetric response in a material. Many can relate to what precautions need to be taken when designing a bridge that will undergo large temperature variations (like in Norway). In each end of the bridge, an expansion joint is built in so that the bridge is allowed to expand/contract without fracturing. Thermal responses are seen in most materials and can be simply explained by the following equations from Fjær et al. (2008):

$$\epsilon_a = -\alpha_T(T - T_0) \tag{4.7}$$

$$\alpha_{T,V} = 3\alpha_T \tag{4.8}$$

Where ϵ_a is axial strain, α_T is the coefficient of linear thermal expansion and T and T_0 are final and initial temperature, respectively. Further, $\alpha_{T,V}$ denotes the coefficient of volumetric thermal expansion in a fluid, as equation 4.7 only considers the axial strain in an elastic rod that is free to deform. If the same rod should be constrained, meaning that it is not allowed to contract/expand, one will cause thermal stress to increase/decrease as temperature increases/decreases. This stress is given as:

$$\sigma_a = -E\epsilon_a = E\alpha_T(T - T_0) \tag{4.9}$$

A thermal response is also something that Kristansen (2015) discussed as a potential method of inducing a formation response, even in combination with underbalanced conditions - Figure 4.10 illustrates this. In the figure, it is clear what mechanisms are

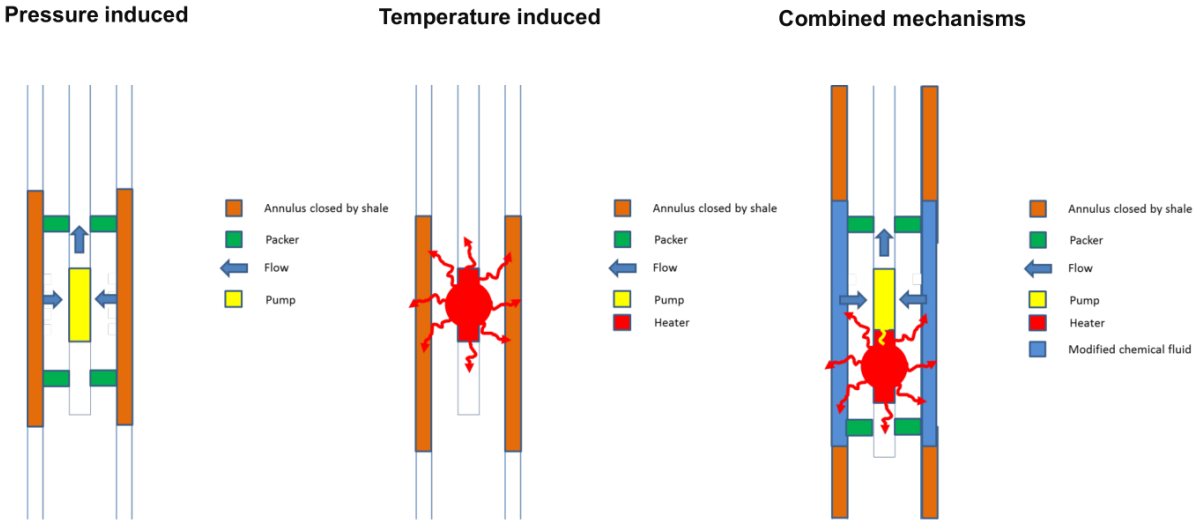

Figure 4.10: *Illustration of different methods potentially inducing a formation response (Tron Kristiansen, BP, 2015)*

proposed as possible methods to induce a formation response - either pressure, temperature or chemical reactions. It should be emphasized that "shale" does not refer to one specific rock type, but a range of rock types who all have in common a high content of clay minerals. Therefore the concepts that are presented here do not necessarily apply to all shales. In addition, equation 4.8 describes volumetric strain in a fluid - however we are interested in describing a similar response in a material with a configuration like that in shale.

Li and Wong (2013) presented a study on thermally induced strain measurements in shale from the Western Canada Sedimentary Basin. In the study it was found clear signs of a dilation/contraction behaviour of the shale depending on whether the temperature had exceeded 65°C or not. Up to that threshold, the material exhibited dilatant behaviour, and opposite after. This behaviour was explained with the Stern layer/Double Diffusion Layer (DDL) theory which, in a simplified way, states that between clay platelets there are several layers of water. The water is bound inside the platelets, but whenever the temperature reaches a certain point, the energy which converts to movement of water molecules turns the bound water into free water that is able to move out of the shale. This results in a shale rock that contracts at sufficiently high temperatures.

Due to the orientation of particles inside shale (sheets in layers upon layers), the strains that are produced when the material is heated differs in the direction perpendicular to the layers compared to the direction parallel to the layers. In their paper from 2013, Li and Wong presents a model of thermally induced strain in shale. Before introducing the expressions, a more detailed description of Stern layer and DDL must be given.

Figure 4.11 taken from Cosenza et al. (2010) displays the different water layers between clay platelet layers in a saturated shale. The Stern layer contains the water that is bound between the platelets. As already mentioned, the amount of free water able to diffuse through the shale increases with temperature, which means that up to a certain temperature level the DDL thickness increases. DDL thickness will start to decrease again as temperature increases at high temperature levels. Taken from Li and Wong (2013), Figure 4.12 is an illustration of the way that shale dilates and contracts when only the thermal effect is taken into account, where the development of Stern layer thickness and Diffusion layer thickness become apparent. In general, this leads us to believe that at very large depths where the in-situ temperature is already considerable, the volumetric response to an increase in temperature induced from the wellbore will not cause any dilatant effect in certain shale types. After considering this, we are ready to introduce relationships from Li and Wong (2013) describing strains in x, y and z-directions where x and y are parallel to the platelet plane while the z-direction is, not surprisingly, the

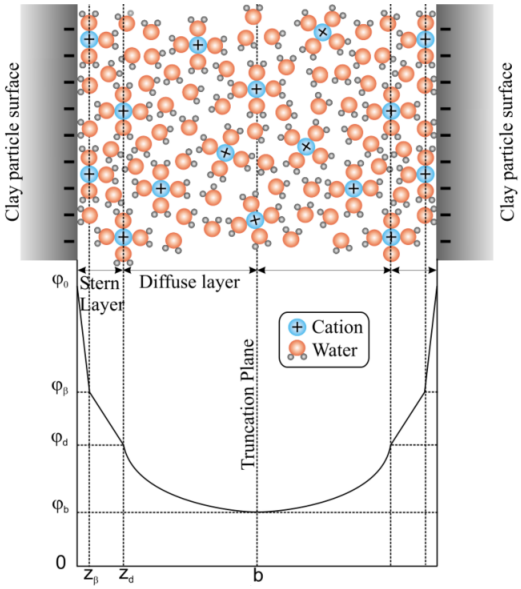

Figure 4.11: *Display of the interlayer bound and free water in shale (Gonçalvès et al., 2010, p. 3)*

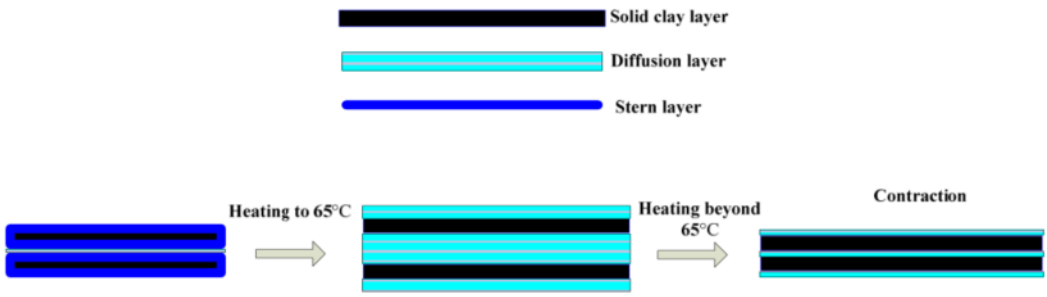

Figure 4.12: *Display of the dilation/contraction due to thermal effect (Li and Wong, 2013, p. 7)*

direction perpendicular to the platelet plane.

$$\begin{aligned} \epsilon_x &= \epsilon_s + \epsilon_{st} n_m + \epsilon_{xd} n_m \\ \epsilon_y &= \epsilon_s + \epsilon_{st} n_m + \epsilon_{yd} n_m \\ \epsilon_z &= \epsilon_s + \epsilon_{st} n_m + \epsilon_{zd} n_m \\ \epsilon_v &= \epsilon_x + \epsilon_y + \epsilon_z \end{aligned} \tag{4.10}$$

In equation 4.10, ϵ_x, ϵ_y and ϵ_z are strains in x-, y-, and z-direction, respectively. Further, ϵ_s is the linear thermal strain in the solid matrix of the shale, ϵ_{st} the strain of the Stern layer, n_m the volume in the pores made up of the Stern and Diffusion layers, ϵ_{xd}, ϵ_{yd}, ϵ_{zd} are the strain components in the DDL's along one of the three directions, and finally the

ϵ_v which is simply the total volumetric strain.

The linear strain ϵ_s in the matrix can be described by equation 4.9. For further details regarding strain calculation in Stern and Diffusion layers, the work by Li and Wong from 2013 is recommended.

4.2.4 Pore pressure alteration

In the cases of both chemically and thermally attempting to induce a formation response, the process of altering the pore pressure and the consequences this has is instrumental. Ideally, the rock is affected in such a way that the effective stress decreases, bringing the rock closer to a failure state - displayed in Mohr-Coulomb's plane strain failure criterion in Figure 4.13. In a P&A-setting, the ideal outcome is that the rock then plastically deforms and creates an annular seal. The effect on the effective stress in the rock is made

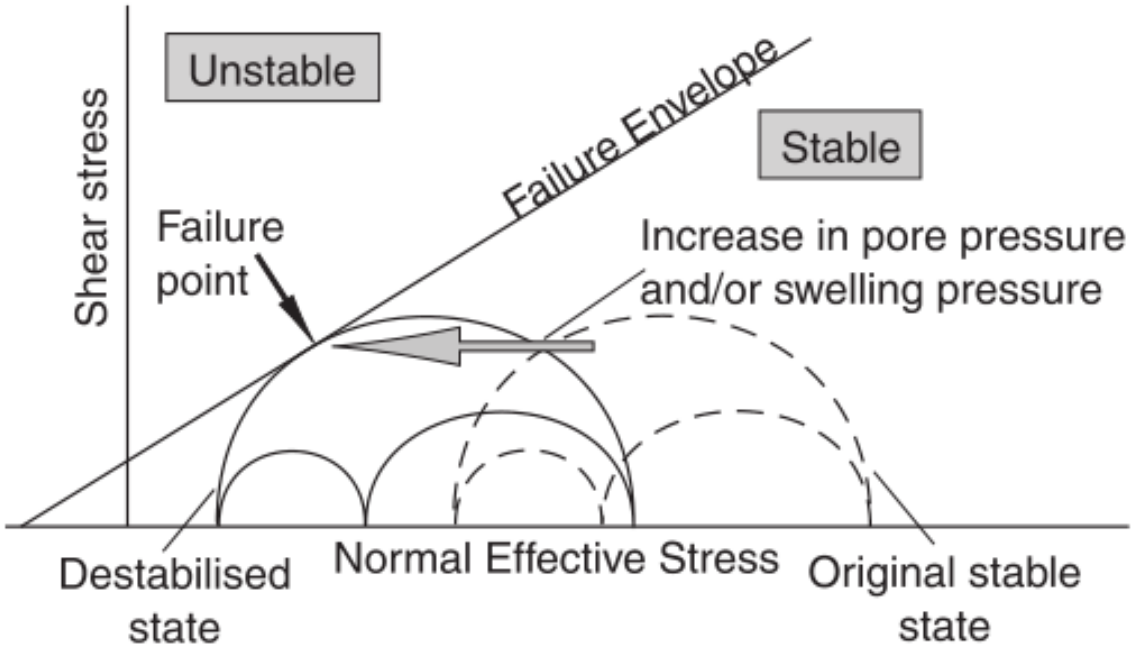

Figure 4.13: *Mohr Coulomb's criterion, description of stress state around wellbore (van Oort, 2003, p. 219)*

clear by equation 4.11.

$$\sigma_{eff} = \sigma_{axial} - P_{pore} \tag{4.11}$$

An effect that is quite intuitive as an increase in pore pressure takes up some of the load from the rock matrix. To what extent the pore pressure can in reality be altered obviously depends on the rock itself. SINTEF has in recent experiments (2018) proved that altering the thermal conditions in a hole by applying heat energy, the pore pressure is indeed affected. The same answers do not yet exist for a chemical stimulation - however it is established from decades of drilling experience that many types of shale are sensitive to certain fluid systems in terms of swelling pressure inside the pore system.

4.3 Shale and cement

Making a comparison between standard Portland cement and a shale with typical properties aids in understanding the difference between the two materials. By using the well established Darcy equation for flow in one dimension, one can make a quick estimate and obtain an indication of the different properties. The Darcy equation in 1-D is given as:

$$Q = -kA\frac{P_1 - P_2}{\mu L} \tag{4.12}$$

Now assume that an annular space outside the production casing is filled with an equally long interval of either Portland cement or a low-permeability shale. If all other input values in 4.12 except the permeability are also assumed to be equal, and the fraction of flow in cement over flow in shale is taken, one is left with:

$$\frac{Q_{cement}}{Q_{shale}} = \frac{k_{cement}}{k_{shale}} \tag{4.13}$$

Assuming a normal permeability value for good Portland cement of 20 μD and a typical value for compacted shale of 20 nD (value obtained from Kristiansen, 2015), one obtains that the flow through the cement is a thousand times higher than through the shale. In other words, an interval of a couple of meters of a low-permeable shale can in theory provide the same seal as a cement plug stretching over several hundred meters.

According to the guidelines in NORSOK D-010, there exist specific requirements for how long each plug should be - a parameter that is obviously hard to control in the case of a

natural shale barrier. However, due to cement's vulnerability to for example sulfuric acids and carbon dioxide, the duration of the integrity of a cement plug is also unclear as these acids are occurring in the underground. In other words, the "infinity-perspective" in the NORSOK D-010 document becomes challenging to account for when establishing a plug. With cement, a common issue is the forming of cracks or micro-annuli between cement and casing. In an ideal ductile shale barrier, it is thought that the formation repairs itself if such damage occurs - making it a perfect sealing alternative that accommodates the requirements/guidelines in NORSOK-D010.

4.4 Real examples

Two wells from real life, in this discussion referred to as 2/4-X and 2/4-Y, are considered. Information and extracts from wireline bond logs have been provided by ConocoPhillips Norway (not available online).

4.4.1 2/4-X

The 2/4-X well on Ekofisk, displayed in Figure 4.15 was used for a slot recovery in 2005 - meaning that the well had been plugged, but by using the same wellhead, a sidetrack was made through the 13 3/8" intermediate casing from which a 11 3/4" liner was installed. After this, the production casing was hung off from the wellhead with a setting depth just above the reservoir. Also, a mid string external casing packer (ECP) was installed above the 11 3/4" liner hanger - a standard solution on Ekofisk.

The ECP contributes to a trapped volume between itself and the production casing TOC. The trapped volume was discussed as a possible contributing factor explaining why the formation did not deform inwards. The same phenomenon is seen in several other wells. However, there are also examples of wells with an ECP apparently causing a trapped volume, but with a very strong formation response on the logs.

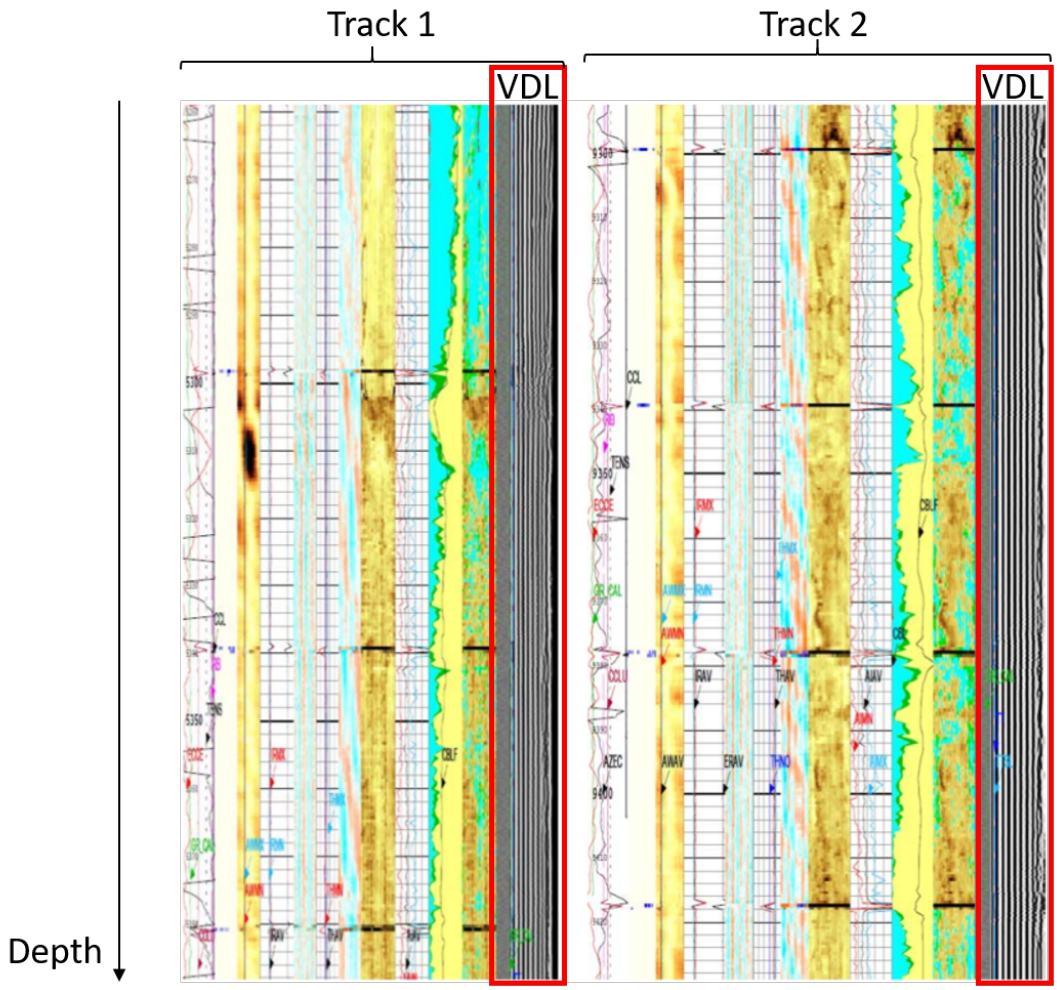

Figure 4.14: *Log readings from well 2/4-X (Courtesy of ConocoPhillips Norway)*

Figure 4.14 is an extract from a wireline log analysis of the 2/4-X. Track 1 is from an interval about 100 meters long directly beneath the 11 3/4" liner shoe. Track 2 is an interval approximately at the depth of the production packer. In both tracks, by looking at the variable density log (VDL) on the far right of each track, one can see that the casing is free hanging with no solid material impinged onto the outside of it. Without going into too much detail about the VDL, it can be interpreted by seeing whether or not there are clear separate white and grey vertical lines in the track (like in Figure 4.14). The principle of the logging tool is to emit acoustic waves and read the returning amplitudes. If the casing is free hanging, the amplitude response is as in Figure 4.14. If not, there is no clear separation between the white and grey area in the track. Thus, one can conclude based on the logs that there are no annular seals in any of these intervals.

The logging operation was performed in 2014, nine years after the initial installation of the sidetrack completion. Also, worth noting is that the production casing interval was drilled with a standard mineral OBM.

4.4.2 2/4-Y

Well 2/4-Y on Ekofisk, wellbore schematic in Figure 4.16, was chosen to undergo permanent P&A in 2016, approximately 25 years after completion. The 12 1/4" section in this well was, opposed to 2/4-X, drilled with seawater based drilling fluid. Moreover, the production casing was hung off just above the reservoir with a low TOC and also an ECP above the intermediate casing shoe, creating a trapped volume between TOC and ECP.

From Figure 4.17, it is clear that this well had long intervals of annular seals above the estimated top of barite (TOB) (which is indicated with a red marker). The "Marker"-column in the track indicates the quality of the bonding in the annulus where dark grey means high quality and light brown means low to no bonding. The trend is unambiguous when all logs (ultrasonic imaging tool (USIT) and VDL) are considered together. There is an interval in the middle where there is no annular seal. It was believed by COPNO that the reason for this was a particularly high occurrence of diatomite, a soft siliceous sedimentary rock, in this interval - lacking the apparent plastic properties of the clay-rich rock above and below it.

In order to take away the essence from Figure 4.17, one can consider the Marker-column and see what areas are marked with grey - those areas have good bond on the outside of the casing, while light brown areas are no-bond zones.

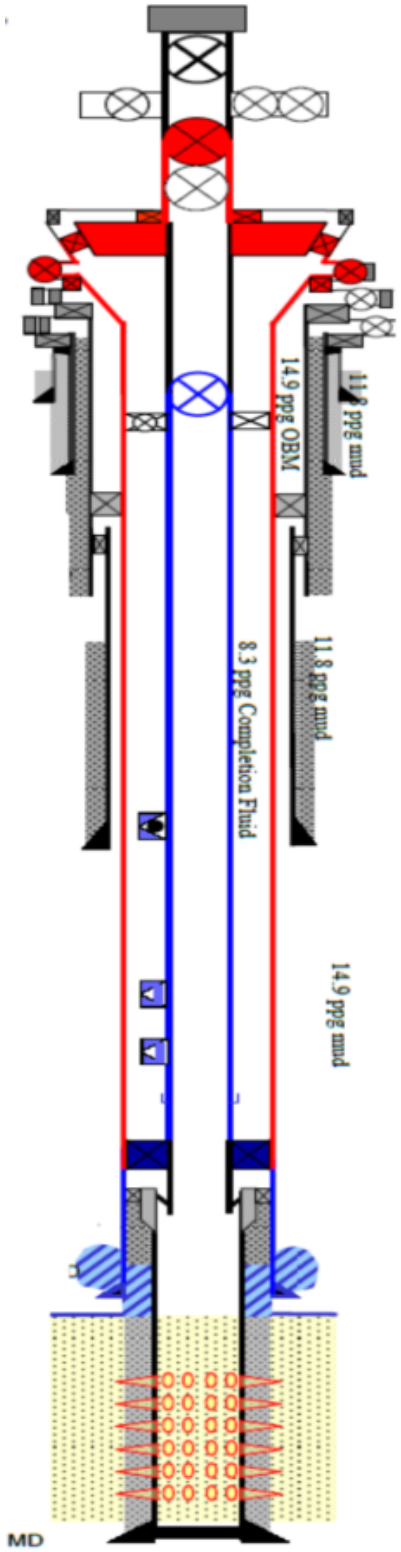

Figure 4.15: *Well 2/4-X(Courtesy of ConocoPhillips Norway)*

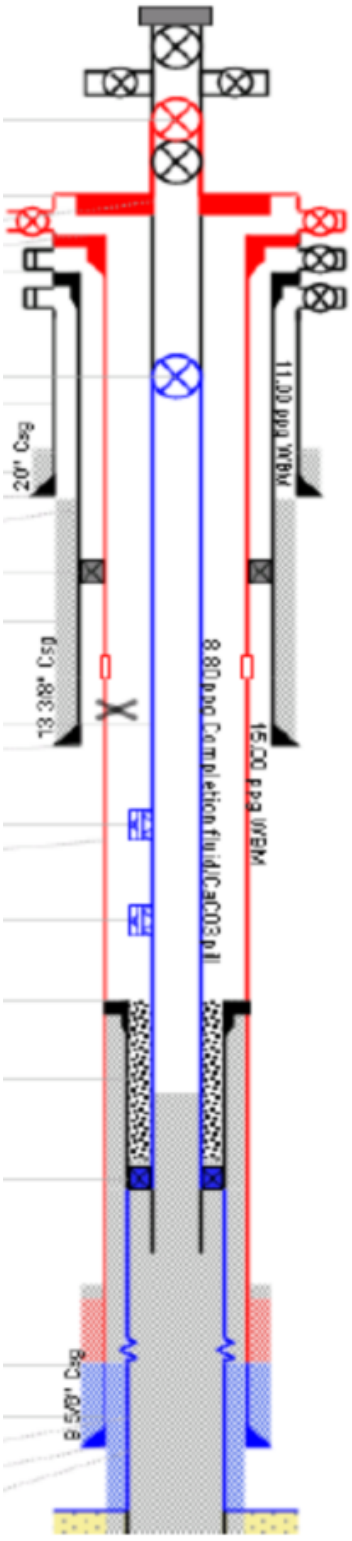

Figure 4.16: *Well 2/4-Y(Courtesy of ConocoPhillips Norway)*

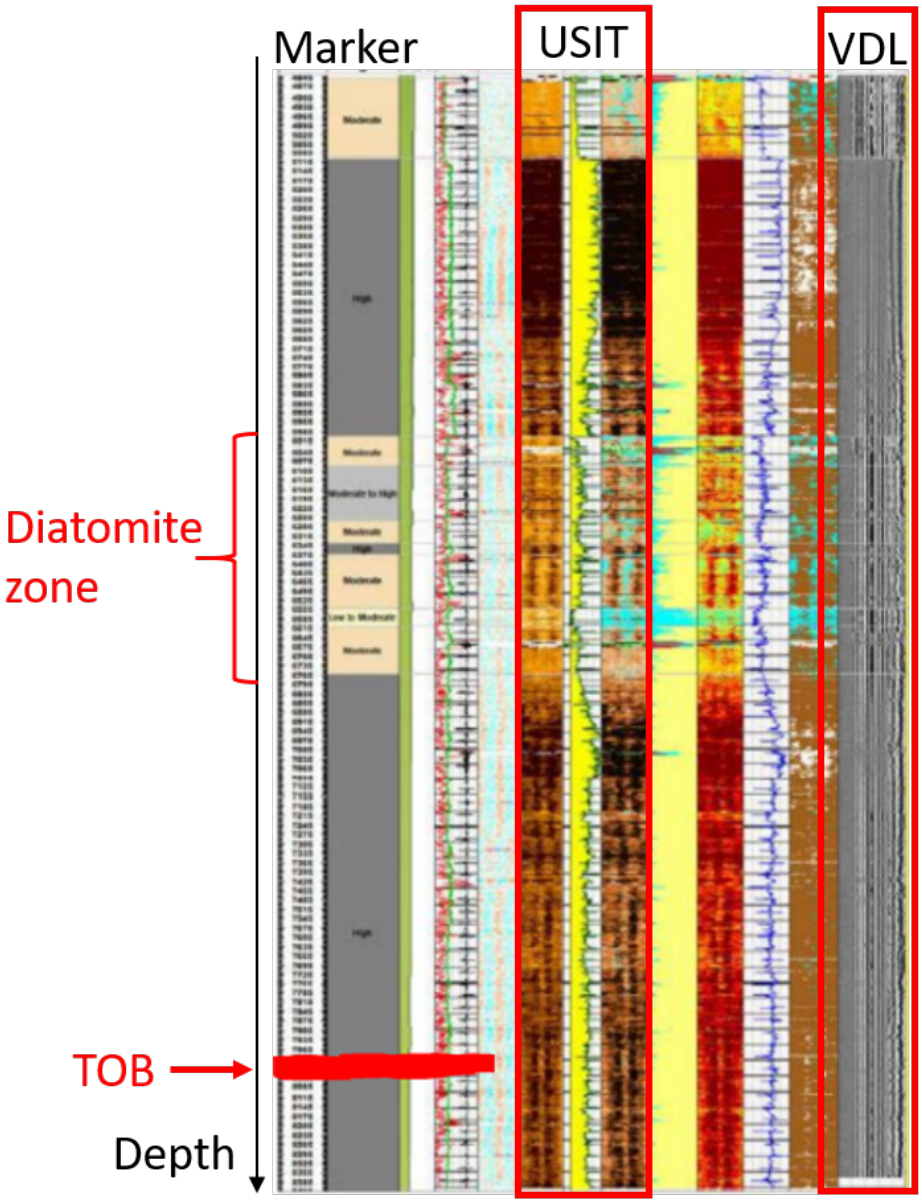

Figure 4.17: *Log readings from well 2/4-Y, red marker indicates estimated top of baryte (Courtesy of ConocoPhillips Norway)*

The transition zone at the top of the track (from light brown to dark grey) is the depth of the 13 3/8" intermediate casing shoe. Thus it is no surprise that the casing is free hanging above that depth - confirmed by both light colored USIT log and a VDL track indicating free hanging casing.

Further, COPNO clearly expressed that they were confident that they did not read cement or settled mud material in the seal zones, but an actual formation seal.

Now, assuming that the trapped volume effect is indeed capable of preventing an inwards deformation of the rock, why has the formation still been able to form a seal in well 2/4-Y? One explanation is that as the formation moved inwards, the increasing pressure was allowed to escape - meaning that the fluid in the annulus leaked off somewhere.

COPNO listed the following possible "routes" for such a scenario:

- Down towards a depleted reservoir
- Into the rock matrix or a permeable layer
- Up the annulus and out a gate valve

Given that normal completion fluid (like that placed above the TOC in the annulus) has low compressibility, it is clear that either the pressure from the inwards moving formation in well 2/4-Y was extremely large - or the fluid has actually leaked off somewhere, the latter alternative supported by the "escape-theory" presented by COP.

4.5 Remarks

We may conclude that shale as a barrier material has already been verified in many cases as good integrity plugs. But to identify such a material, more data is needed. Now, this project has in addition to performing a literary review, also consisted of experiments in the laboratory where permeability- and P-wave-velocity measurements in sand/clay mixtures and natural shale material have been carried out. The results give more insight between relations and trends in a possible barrier material, some of which are different than what was expected beforehand.

Before presenting the results from the experiments, a closer look at the experimental and analytical methodologies is presented in the following chapter.

5 Experimental and Analytical Methodology

Obtaining data from transient permeability tests in the laboratory was performed by going through a step-wise procedure where all steps were documented and performed identically in all tests. Before any of the testing could commence, all equipment had to be calibrated.

In 2009, Mondol performed a study on silt-kaolinite mixtures that has served as part of the inspiration in the current project. He acknowledged that the prediction of relevant properties like porosity and permeability in clay-rich rocks is a challenging task - which gave rise to his study on how these two properties develop in different silt-kaolinite mixtures. A part of this project has also been to perform tests on such mixtures, although with some differences: The current project applied a quartz grain size between 355μm and 230μm - which is considerably larger than in Mondol's case (4-40μm). Also, powdered smectite as well as two naturally occurring shales, Pierre shale and Sele equivalent shale, have been tested in the laboratory. In 2017, Oftedal performed experimental work on quartz-kaolinite mixtures. The results from that study are included in this report.

A mathematical model presented by Reuschle (2011) was established and applied for the analysis of all the data points that were obtained. This section aims to provide an overview of the entire process from beginning to end.

In addition to permeability and porosity data, measurements from an ultrasonic tool reading the travel time of compressional waves were also performed. The methodology for this will be presented in its own section while all the relevant results are presented in Chapter 6.

5.1 Physical set-up

The test rig was made up by several components, all of which are described in the following sections. In addition to presenting the equipment itself, the mathematical procedure behind certain calculations is also presented where it is relevant.

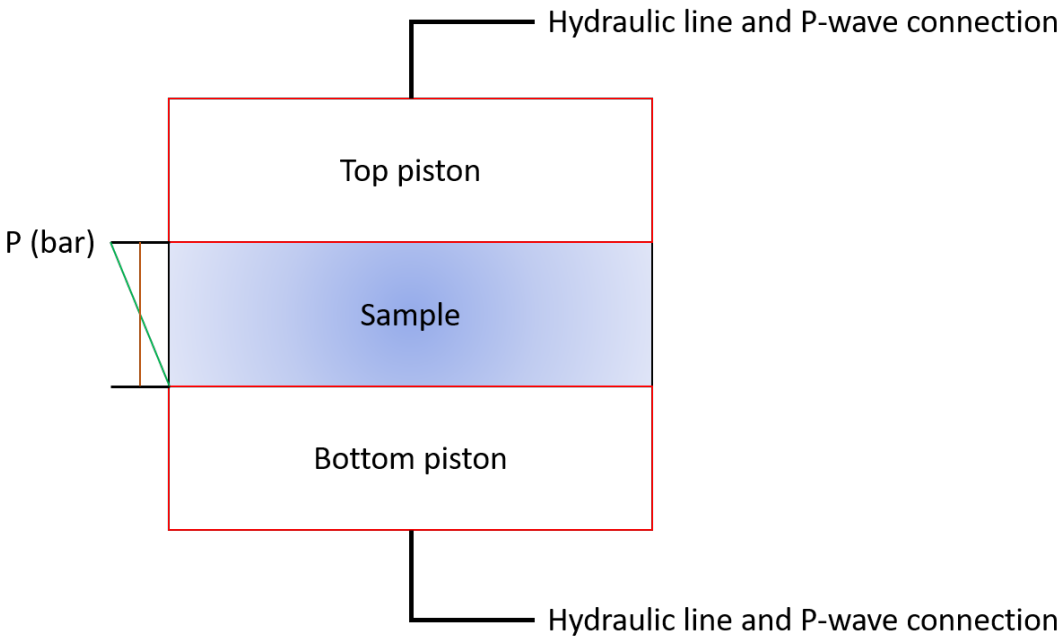

Figure 5.1: Test cell schematic

First, a sketch of the test cell in which the rock samples were placed should be considered in some detail, a schematic is shown in Figure 5.1. The cell was a thick-walled cylinder with an internal diameter of 38mm. Further detail will be given later, but the practical benefit of the cell can be seen by considering the schematic of the test cell. The sample that was tested was placed between two pistons with internal lines that ensures hydraulic communication throughout the system. When a transient test was performed, the principle of the test was to induce a pressure increase by decreasing the pore fluid volume in the circuit above the sample and to induce a pressure decrease below the sample by increasing the volume in the pore fluid volume in the circuit. The green pressure gradient visually illustrates the beginning of such a test, and the brown line pictures the situation when system is in equilibrium with normal pore pressure (pressure of 2 MPa throughout the sample).

Deadweight frame

In order to expose the rock samples to varying loads, a deadweight frame with a loaded moment arm was applied to create enough axial load. No hydraulic pressure device

was available which made the deadweight frame a favorable choice for these particular experiments. The principle of the frame is quite simply to use the moment arm to create a large axial load (up to 20 MPa in this case) on the sample using a relatively small amount of weight plates. Figure 5.2 displays a sketch of the set-up with the most essential components included. From the equation

$$M = FL, \tag{5.1}$$

the moment around the hinge point can easily be obtained using L_{arm} and the force

$$F = mg, \tag{5.2}$$

which is the gravitational component resulting from the product between mass of the deadweight m, and the gravitation constant g.

Now, because the sample undergoes a relatively large axial strain, especially in the case of high clay content samples, the moment arm will never be in a completely horizontal position except of course in a single point in time. Therefore, one has to account for this when calculating the resulting moment by decomposing the vertical force into an x-component (F_x) which is parallel to the moment arm and a y-component (F_y) which is perpendicular to the moment arm:

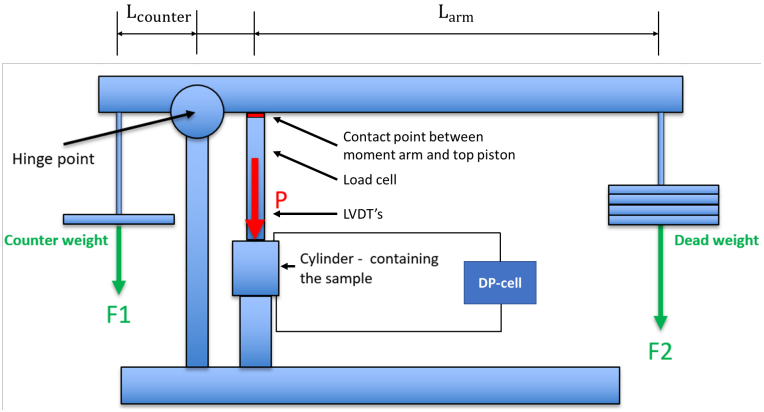

Figure 5.2: *Deadweight frame*

$$F_y = F_2 cos(\alpha_F) \tag{5.3}$$

The perpendicular component found from equation 5.3 is the one that must be applied

when finally calculating the moment around the hinge. In the equation, α_F denotes the angle between the vertical force component and the horizontal force component. This is included because the rod from which the deadweight is hung is not totally fixed in the moment arm, but hinged so that the deadweight rod is always in a vertical position.

Of course, the moment arm itself has to be considered as well because it is a hollow, but relatively thick-walled piece of steel and represents an addition to the moment created around the hinge point due to its own mass. Assuming that the moment arm has equal dimensions (width, height, thickness), equation 5.4 displays how to calculate the moment from the arm itself (dividing by 2 is done because of the assumption of equal dimensions throughout the arm length).

$$M = \frac{FL_{arm}}{2} \tag{5.4}$$

By using the same principles, the resulting negative moment created by the counterweight can also be easily calculated. The counterweight has remained the same throughout all the tests and has no other practical value than to make it easier to lift the arm when unloaded.

The deadweight frame provides axial load on the sample, however there are also several other important components in the system.

Regarding temperature variations in the laboratory and the effect this has on the length of the arm - this is a factor that may be taken into consideration, but the assumption was made that due to small temperature variations it was neglected. A quick calculation can be performed to "verify". By assuming a linear thermal coefficient of expansion in steel of $0.000012\frac{m}{m\,\deg C}$ (from Callister and Rethwisch, 2014 p. 789), length of the moment arm 1.2 meters and a maximum temperature variation of $2.0\deg C$, one obtains:$\Delta L = 1.2 * 0.000012 * (2)m = 2.88 * 10^{-5}m$. Thus a change in moment arm length of roughly 30 μm might occur - in other words negligible for all practical purposes in the current project.

Pore pressure pump

A pump was used to maintain constant pore pressure in the sample, thus reducing the effective stress on the test sample. One of the most important reasons for using the pump to apply a pore pressure is to ensure that the axial load is distributed equally across the entire area of the sample inside the cylinder. It also provides a much better control of the fluids in the system that is connected to the sample via a differential pressure transducer.

The pump has two separate pistons working in pair which ensures that any pulses in the system are kept to a minimum as it is able to refill with one piston while the other one keeps the pressure. With a pressure capability up to 20 000psi (in excess of 137 MPa), the pump delivers more than enough - given that the pore pressure in all tests has been limited to 2 MPa.

The pump collects the pore fluid (3.5 weight-% sodium chloride) from an external reservoir and applies the fluid when maintaining the pressure in the system. The pump is reliable in terms of maintaining pressure and avoiding unwanted pressure pulses, but relatively fragile and requires a good operating routine regarding shifting between different pressure and rate modes so that the moving pistons do not go stuck in an extended position - leaving the pump useless.

Differential pressure transducer

The differential pressure transducer (DPT) was a critical part of the project as it was used to determine at what rate the pressure over the sample reached equilibrium when performing the permeability tests, more about that in the section regarding the data acquisition.

The DPT was the link between the pore pressure pump and the cylinder containing the sample. It was lined up to two air-pressurized valves that allowed closing and opening of the system against the pump without altering the volume inside the pipes, which was necessary to avoid any unwanted pressure pulses. The fluid circuit with the DPT also contained two needle valves. The needle valves directly affected the system volume when

turned, and because the total volume in the pipes above and below the sample was so small, only a slight turn of the needle valves were necessary to induce a differential over the sample which was large enough.

Before experiments began, the DPT was calibrated by connecting one side of the cell to the pore pressure pump while the other side was left open to atmospheric pressure. This allowed the user to increase the pressure using the pump and then tabulate each pressure value with the electric signal transmitted by the cell.

Pistons

The pistons were located inside the cylinder with the sample between them. They had an interior line which drained fluid passes through as well as well as the possibility to connect with the sonic tool to do travel time measurements through the sample.

At the end of the pistons, two types of filters were fastened using silica gel. At first a paper filter, then a solid aluminium filter on top. The silica gel was allowed to dry one day before the actual test began. Obviously the filters were crucial in order to avoid that solid material went out along with the drained water, something that was particularly challenging during the tests on the quartz/smectite samples because of the very small particle size of the clay. However, it was fully possible to avoid when the filters were fastened properly and did not cause any problems in the tests. This was easily verified when a test was done - if there was clay residue in the circuit fluid outside of the cylinder, then a leak had occurred.

To be able to read differential pressure, the top and bottom piston were connected to the pore pressure pump via the DPT-cell - one piston connected to each side of the cell.

P-wave transmitter and transducer

The equipment used to measure travel time consisted of a transmitter/receiver and a signal amplifier as well as a computer used to operate the tool.

The apparatus was used to transmit P-waves (compressional waves) through the system and subsequently collect the wave velocity in the rock sample.

A picture of the equipment can be seen in Appendix A.

Force transducer

The force transducer was a 100 kN strain gauge cell located between the top piston and the moment arm. In order to determine the axial load on the sample, the force transducer was important because the calculation of total axial load on sample was done by using the reading from the force transducer and applying $\sigma = \frac{F}{A}$.

The force transducer was calibrated before the experiments. Using the principles from equation 5.3 and 5.4, the force on the transducer was correlated to the deadweight hung from the moment arm. Of course the distance between the hinge point and the contact point between the moment arm and piston had to be accounted for. As with the DPT, all values were tabulated and coupled with the respective electric output signal.

Temperature and pore pressure transducers

Connected to the cylinder with the sample was also a temperature transducer and a pore pressure transducer. These were mainly included so that control of temperature and pressure was maintained. Any fluctuations would have an impact on the dynamic viscosity of the pore fluid, thus the temperature at any test was accounted for when calculating permeability - more about this in section 5.4.

5.2 Test sample

Before performing each test on the synthetic rock materials, a relatively rigorous process of preparing the rock sample was necessary to obtain a good and homogeneous mix of the brine, quartz and clay mineral (kaolinite or smectite). A different approach had to be taken with the natural shale material.

5.2.1 Synthetic samples

The process began by calculating the mass of quartz and kaolinite/smectite to be included in the mixing beaker based on a volumetric ratio - not a mass ratio. When the solid material had been weighed up and placed in a separate container, the process of mixing the materials with water could commence. It was important to add only a little bit of solid material and water at a time in order to avoid any unwanted clumping of the material - a phenomenon that easily occurs when the clay content is high and gets in contact with water. When all solid material for the mix had been used, it was up to judgment to assess how volatile the "slushy" mix was before it could be poured into the cylinder for testing. If to sluggish, then some more brine was added to make it easier to work with.

In the process of mixing the material, it was important to maintain control of all the equipment that was involved. This was necessary to be able to know how much mass of each material had been put inside the test cylinder.

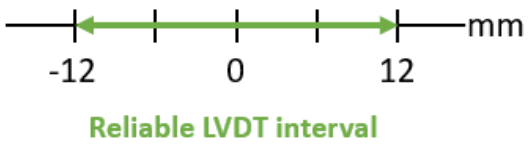

Figure 5.3: *Reliable interval of LVDT's*

Before any test would start, it was necessary to "pre-drain" the test sample for any excessive water volume. The reason is that the linear variable displacement transducers (LVDT) were only reliable within a certain interval. Therefore, the samples could not be allowed to compact more than a certain length when the LVDT's were applied (during the actual test) (see Figure 5.3).

To get a better understanding of how the grains were distributed in the samples after the mixing was done, CT-scans were done on some of the samples. In Figures C.2 (50% kaolinite, 50% quartz) and C.3 (50% smectite, 50% quartz), two slides from the scan are displayed, giving a clearer picture of the grain distribution. Also, these figures served as a confirmation that the mixing of the powdered clay minerals was well performed without any major clumping of the clay material in the sample.

5.2.2 Pierre Shale

The Pierre shale used in the experiments had initially been stored in mineral oil before the sample was acquired. The process of preparing the Pierre sample was to crush the sample in a mortar until the particles were relatively small - visually inspected. Then, the material in the mortar was sieved through a 1mm aperture sieve - thus excluding all particles more than 1mm. After a sufficient amount of shale had been crushed, the material was weighed accurately and mixed together with the same pore fluid as in the synthetic samples (3,5% NaCl brine).

Due to the large grain sizes in the Pierre shale samples, the external surface area (m^2/g) is much smaller than in the powdered synthetic materials and the mixing with water required much less time.

The Pierre samples were, like the synthetic samples, pre-drained for excessive water before starting the test.

5.2.3 Sele shale

The Sele equivalent shale was prepared in a similar manner as the Pierre shale. Being much more ductile and easily shaped by exerting a force to it, a sample was divided into pieces and put into the cylinder - mixed with brine. Then, the sample was set to compact under a compaction load of 2 MPa for 2 hours to remove all air and excessive water in the sample.

5.3 Transient Permeability Test

Figure A.1 in Appendix A displays schematically how the sample is in communication with the differential pressure transducer and the pore pressure pump via air-pressurized valves.

To test the transient permeability in the sample, a step-wise approach was followed:

1. Closed air-pressurized valves to isolate the DP-cell from the pore pressure pump

2. Turned needle valves approximately one quarter of a full round in order to generate a pressure differential over the sample that was sufficiently large

    - This caused a volume change in the system that created a pressure pulse over the sample - because the system volume was so small

3. The system remained closed against the pump until pore pressure over the sample reached equilibrium (DP=0)

4. The system was re-opened by opening air-pressurized valves and the needle valves were turned back into original position as small volumetric changes no longer affected the system pressure

This procedure was performed four separate times in each test:

What	**Value (MPa)**			
Axial stress	5	10	15	20
Pore pressure	2	2	2	2
Effective stress	3	8	13	18

Table 2: *Pressure regime of the four transient permeability tests*

5.4 Data processing

The tests that were performed produced quite large datasets from which only the essential data points were extracted and analyzed to obtain the relevant properties in the rock samples. As mentioned before, the transient permeability values were calculated using a model taken from Reuschle (2011), who did similar tests on real samples to determine how the permeability is affected by depth (compaction).

The procedure from Reuschle (2011) is based on a mathematical model developed by Bredehoeft et al. (1981), a model that describes how to analytically obtain transient hydraulic properties in tight rocks. The full derivation of the model goes beyond the scope of this text, but the reader can take a closer look at the work by Bredehoeft et al. (1981) to obtain the full picture.

The model includes a few assumptions regarding the compressive storage volume in the sample compared to that in the fluid circuit. A justification of these assumptions can be found in section 6.2.3.2 as this section aims only to describe the methodology.

5.4.1 Transient permeability

The transient permeability has been calculated based on a few assumptions. First of all, it has been assumed that the compressive storage (m^3/MPa) inside the sample (C_s) is negligible compared to the compressive storage in the pore fluid circuit - which is made up of the storage in the upstream line (C_u) and in the downstream line (C_d). (Note that the use of the terms "upstream" and "downstream" does not mean that there is a one-way flow of the pore fluid. The fluid is allowed to escape from the sample both ways during compaction. Upstream and downstream in this context simply refers to the up-side and the down-side of the sample.)

The above assumptions allow for an exponential approximation of the differential pressure decay over the sample, where the decay time is inversely proportional to the sample permeability as shown in equation 5.5 from Bredehoeft (1981), rendered by Reuschle (2011).

$$\Delta P_{pore} \propto exp(-\alpha t) \tag{5.5}$$

Further, equation 5.6 from Bredehoeft (1981) shows the relationship used to calculate the exponential coefficient, α.

$$\alpha = \frac{Ak(C_u + C_d)}{\mu L C_u C_d} \tag{5.6}$$

Where in addition to the compressive storage, the symbols are defined as follows:

t: time

L: sample height (m)

A: total flow area (m^2)

k: permeability (m^2)

μ: pore fluid viscosity (Pa·s)

Further, the position at the bottom of the sample and at the the top are given by $x = 0$ and $x = L$, respectively, where $P_{x=0}$ and $P_{x=L}$ are pressures at sample top and bottom, respectively. The pressure in the upstream fluid circuit is given by P_u and in the downstream circuit by P_d - and time is given by t, then the following conditions for the pressure as a function of position and time ($P(x,t)$) apply for each test:

$$P(x,0) = P_{pore} = 2MPa$$

$$P(0,t) = P_d(t)$$

$$P(L,t) = P_u(t)$$

A change in upstream/downstream pressure was induced at the start of each test and was recorded by the DP-cell.

Practically, the flow area, time and length were easily obtained by measurement. The dynamic viscosity however was not that straight-forward. In the experiments, 3,5% NaCl water was used as pore fluid. Çengel and Cimbala (2014) provides a simple approximation of viscosity in liquids:

$$\mu = a10^{\frac{b}{T-c}} \tag{5.7}$$

Where T is absolute temperature (T=T(°C)+273.15) and a, b and c are experimentally determined constants. However, equation 5.7 does not account for salinity of the fluid. Not surprisingly, an increasing salinity causes a higher viscosity - therefore a relation from Batzle and Wang (1992) that accounts for saline water in temperatures below 250°C was used in the estimation of dynamic viscosity:

$$\mu = 0.1 + 0.333S + (1.65 + 91.9S^3)e^{-[0.42(S^{0.8}-0.17)^2+0.045]T^{0.8}} \tag{5.8}$$

Where S denotes the salinity (ppm/10^6) and T is the temperature in degrees celsius ($\deg C$). This yields a pore fluid dynamic viscosity of approximately 1.074 cP at 20°C. Only very small temperature fluctuations occurred during the tests, having no considerable impact on the results. From Figure 5.4 it is evident that the temperature remained some place around 19°C. Figure C.1 in appendix C displays a standard correlation be-

tween water viscosity, temperature and salinity (Matthews and Russell, 1967).

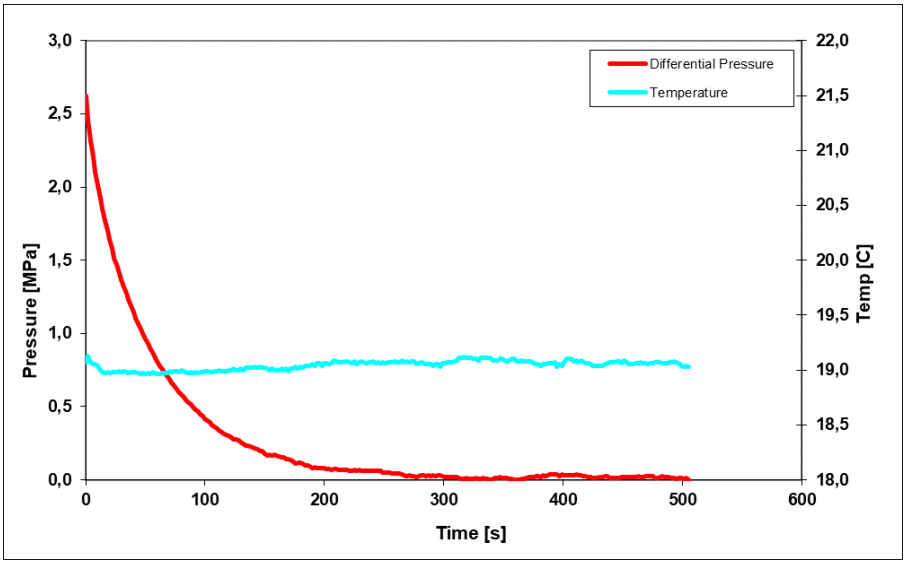

Figure 5.4: *Differential pressure development in a random sample and temperature during same period*

The actual development of the differential pressure from Figure 5.4 is plotted on a semi-logarithmic scale with an exponential trend line in Figure 5.5, while equations 5.5 and 5.6 taken from Bredehoeft et al. (1981), rendered by Reuschle (2011), are used to acquire estimates of the desired properties. In addition to the viscosity, the compressive storages,

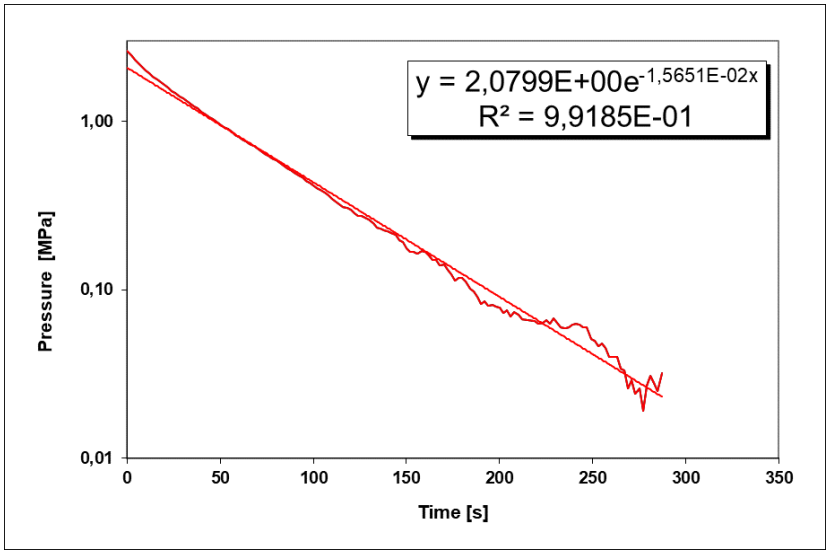

Figure 5.5: *DP trend on semi-logarithmic scale with exponential trend line*

C_u and C_d are found by applying equation 5.9.

$$C_{u,d} = \frac{V_{u,d}}{c_w} \tag{5.9}$$

Where $V_{u,d}$ is the upstream/downstream volume and c_w is the isothermal compressibility of the pore water. The upstream/downstream volumes were determined by emptying the pore fluid circuits before reconnecting to the pump and measuring exactly how much pore fluid volume were stored in each of them by means of pumping at a very slow rate until the lines were filled.

The compressibility of the pore water with a pore pressure of 2 MPa was determined by an interpolation between compressibility values of 0ppm and 100,000ppm NaCl in distilled water taken from Carlson (2003). This yielded a pore fluid compressibility of $4,9813 * 10^{-6} Pa^{-1}$ - a value that is used throughout the experiments described in this report.

In other words, there were mainly two factors that had to be accounted for when using equation 5.6 to estimate the permeability, namely the viscosity and the compressive storage volume. By rearranging equation 5.6, one obtains for the permeability:

$$k = \frac{\alpha \mu C_u C_d}{A(C_u + C_d)} \tag{5.10}$$

Which is the relation used to estimate permeability in all experiments throughout this project.

After each test, the time interval in which the actual permeability measurement was performed had to be determined. Readings of experimental data were performed with a frequency of 1Hz as a higher frequency would have yielded unfavorably large datasets. After doing so, plots like in figures 5.4 and 5.5 were constructed to obtain the α-coefficient used to calculate the permeability.

5.4.2 Travel time and acoustic impedance

In order to obtain more information (and verification) on the degree of compaction, primary compressional wave (P-wave) travel time was measured in the samples that were tested in the experiments. Travel time measurements were taken every 10 minutes throughout the length of the test.

The travel time data were obtained with a different apparatus and computer than what was used for obtaining all other values, therefore the two datasets had to be calibrated with regards to time to make sure that relevant travel time measurements were picked instead of travel times when the sample had not been fully compacted.

After each experiment was done, the data were collected and uploaded to an external computer. From there, the processing of the data was done by using a MATLAB-script provided by SINTEF Petroleum.

The principle of the calculation was to initially measure the system travel time (Δt_{system}) - that is the wave travel time through all the equipment when no sample was in place with the pistons in contact with each other. Then, when measuring total travel time (Δt_{total}) during the tests, any additional time to the system travel time was used as the travel time through the sample itself (Δt_{sample}):

$$\Delta t_{sample} = \Delta t_{total} - \Delta t_{system} \tag{5.11}$$

The travel time has been an additional parameter that was not included in the experiments conducted by the author in 2017. The reason was mainly to obtain more relevant data from the samples that underwent the testing regime described in section 5.3. Regarding the verification of potential shale barriers from wireline logs, this is especially interesting as the travel time in the annulus material tells a lot about what it is that is present. High P-wave velocity normally indicates a material that is compacted, dense and with high stiffness, according to the relation $v_P = \sqrt{\frac{C_s}{\rho}}$, where v_P is compressional wave velocity, C_s a measure of material stiffness and ρ the density of the material. That relation tells us that a high density material does not necessarily show a high P-wave

velocity on the logs, something that may confuse if one is not aware of that fact.

After calculating the P-wave velocity in all materials, using equation 5.4.2 the acoustic impedance in all the materials were obtained.

$$Z = \rho v_P \tag{5.12}$$

When using acoustic logging tools in a well to identify annular material, acoustic waves are transmitted and received by the tool. The data are then correlated with density data and the acoustic impedance, Z, is calculated. Acoustic impedance is a property which is found in all types of material, basically describing how much resistance a wave encounters when propagating through the material in question. Therefore, we are not only interested in the velocity a wave has through the material being tested, but the resulting impedance - giving more information on how such materials would behave in these types of logs.

5.4.3 Porosity

The initial porosity (ϕ_i) of the sample was calculated using equation 5.13.

$$\phi_i = \frac{V_{t,i} - (W_s/\rho_s + W_c/\rho_c)}{V_{t,i}} \tag{5.13}$$

Where $V_{t,i}$ is initial bulk volume, W_q and W_c are dry masses of quartz and clay, respectively, and ρ_s and ρ_c are the densities of dry sand and clay, respectively. Clay refers to either montmorillonite or kaolinite, depending on which one was used in the test. By using initial porosity and the strain caused by the axial loading and measured by the the two LVDT-cells, the porosity in the sample was estimated by equation 5.14.

$$\phi = \frac{V_{porefluid}}{V_{total}} (= \frac{V_{total} - V_{solids}}{V_{total}}) \tag{5.14}$$

The LVDT's provided reliable measurements on how much the sample was compacted in each test from the time of initial application of axial load until end of test.

This method of estimating the porosity is based on an important assumption - namely

that the grains in the mixture are incompressible. That leads to the conclusion that any volumetric change of the sample due to drained pore fluid results in an equal change of the total bulk volume.

In addition to being an interesting parameter, good porosity calculations were important when the density of the rock samples were estimated. Reliable density values were important when processing travel time data and calculating the acoustic impedance.

6 Results and Discussion

In the autumn of 2017, the author (Oftedal, 2017) conducted similar experiments to the ones in the current project, but only on certain quartz-kaolinite mixtures, all tests (and when they were performed) are showed in Table 3.

Kaolinite	**Smectite**	**Pierre**	**Sele**	**Quartz**	**Year**
1.0	0.0	0.0	0.0	0.0	2017
0.70	0.0	0.0	0.0	0.30	2017
0.60	0.0	0.0	0.0	0.40	2017
0.50	0.0	0.0	0.0	0.50	2017
0.40	0.0	0.0	0.0	0.60	2017
0.30	0.0	0.0	0.0	0.70	2017
0.20	0.0	0.0	0.0	0.80	2018
0.10	0.0	0.0	0.0	0.90	2018
0.0	0.75	0.0	0.0	0.25	2018
0.0	0.50	0.0	0.0	0.50	2018
0.0	0.40	0.0	0.0	0.60	2018
0.0	0.0	1.0	0.0	0.0	2018
0.0	0.0	0.0	1.0	0.0	2018

Table 3: *Material compositions in experiments (volumetric ratio)*

The results from the 2017-tests are included in this report with the purpose of extending those results with the newly acquired data.

A pore fluid compressibility of $4,9813 * 10^{-6} Pa^{-1}$ and a dynamic viscosity value found from equation 5.8 were applied. Table 3 also shows the different ratios that were tested with smectite and the natural shale materials. In Appendix B, tables with a complete overview of all the most relevant properties can be found. In this section, a more visual approach with plots and discussion of plots is chosen.

Before considering the results further, note that the lines between each actual datapoint are included mostly for visual aid by connecting the different datapoints. Although the lines may more or less represent the development between each point, it is not certain that it represents reality - a definitive answer can only be obtained by doing more tests and obtaining more datapoints.

6.1 Results from tests

6.1.1 Transient permeability vs clay content

The transient permeability was measured in different sample compositions: quartz-kaolinite, quartz-smectite, Pierre shale and a Sele shale equivalent.

Results are presented according to the materials in the samples.

As expected, the various axial loads and material content in the samples had considerable impact on the properties of interest.

6.1.1.1 Quartz-Kaolinite

This section presents the results from experiments on the quartz-kaolinite mixtures. As already stated, only the 10%- and 20%-kaolinite samples have been tested in the current project. However, data from 2017 are adjusted with new, and more correct, physical properties.

Mondol (2009) presented results on quartz-kaolinite samples which are used for comparison with the results from this project, seen in Figure 6.1. Not surprisingly, there is an obvious decreasing trend as the kaolinite content and compaction load increase. Mondol (2009) discovered a considerable drop in permeability in all the samples with 50% kaolinite content. A similar trend was seen in the current project, but with the drop occurring at 40% kaolinite instead of at 50%. There was also a drop for a certain clay percentage in the porosity measurements, more about this in section 6.1.1.2.

As the kaolinite content increased, there was an indication that the permeability decreased in larger steps, seen when moving to the right in Figure 6.1a.

Vertical permeability in the current project had a strong trend of having considerably lower values than in the case of Mondol (2009) - seen when comparing numerical values from the two cases.

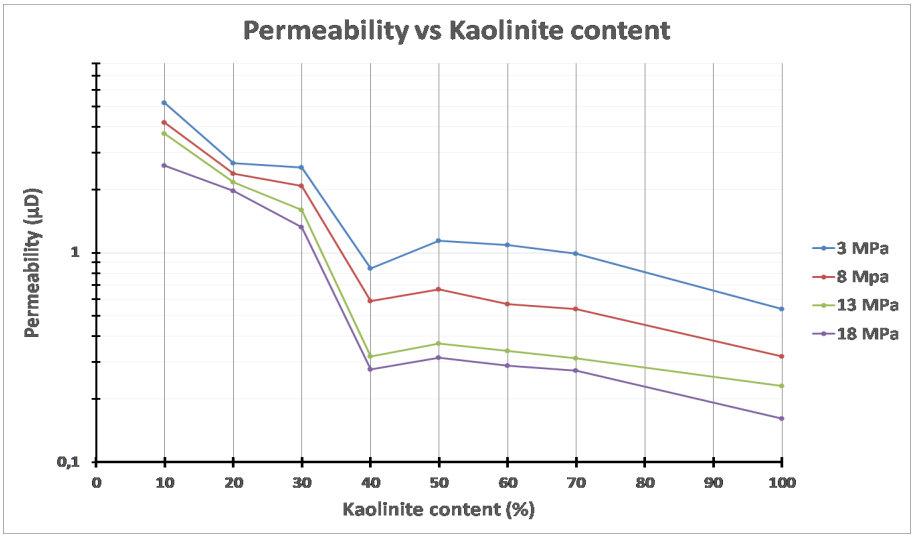

(a) *Current project*

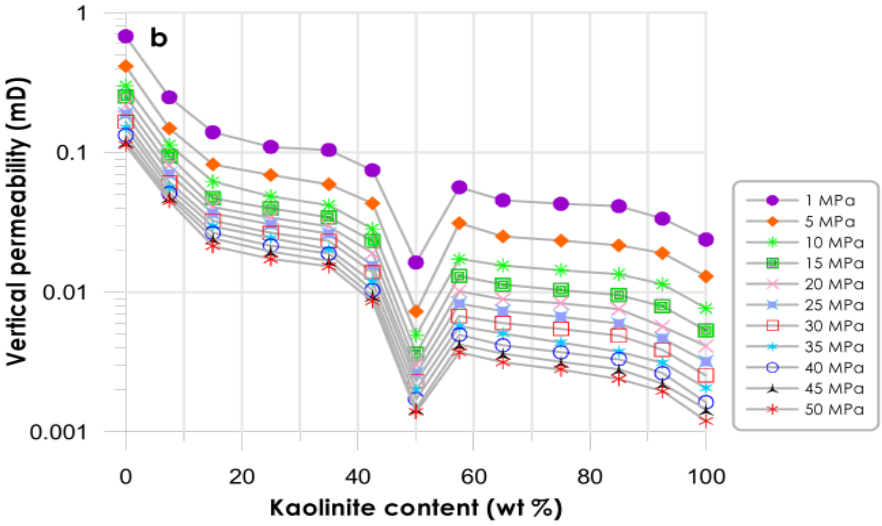

(b) *Mondol (2009, p. 2142)*

Figure 6.1: *Comparison of permeability measurements*

6.1.1.2 Quartz-Montmorillonite

Prior to the experiments with the smectite samples, it was expected that a considerable effect on permeability would be observed. The notable difference in particle size is an important explanation as to why this was expected, outlined in Table 1.

From the results that were eventually obtained, it was clear that there is a considerable difference between kaolinite- and smectite-dominated samples - namely that the induced pressure pulse requires considerably longer time in smectitic samples to let the pressure

reach an equilibrium. Clearly seen in Figure 6.2, the permeabilities in the smectite

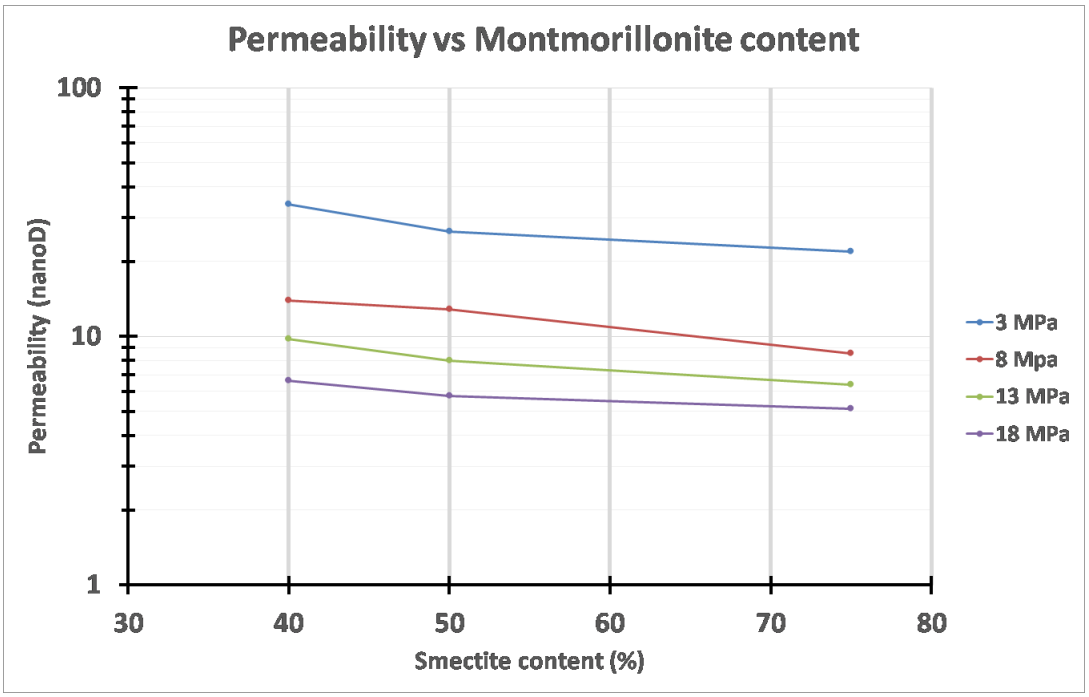

Figure 6.2: *Permeability (nD) vs montmorillonite content*

samples are in a different range of values (lowest of 5 nD in the 75% smectite sample) compared to the kaolinite-samples where the lowest permeability was calculated as 161 nD in the pure kaolinite sample with no quartz present. The differences in permeability from 3 MPa to 18 MPa effective axial stress are not very large. Clearly, even at the lowest smectite content and at 3 MPa axial stress, the sample displays very tight properties. Note that he decrease is visually somewhat "dampened" and does not look very dramatic due to the semi-log plot.

6.1.1.3 Pierre and Sele shale

The Pierre and Sele samples showed similar trends in permeability compared to the other materials - a decreasing trend was clear, seen in Figure 6.3. In the Pierre shale, the tight properties of the material did not fully show until the sample had been consolidated under the three highest axial loads, clearly seen by the drop in Figure 6.3. After being compacted by 3 MPa, the permeability was calculated to be in excess of 200 nD. After the last compaction step of 18 MPa effective axial load, the permeability was down to

12 nD. It was expected to see a considerable decrease in permeability after the samples were compacted under higher efficient stress than 3 MPa, which was the first load of the compaction steps. The reason for that expectation was that the large grain sizes that initially made up the sample (before compaction) would maybe allow for flow paths through the sample.

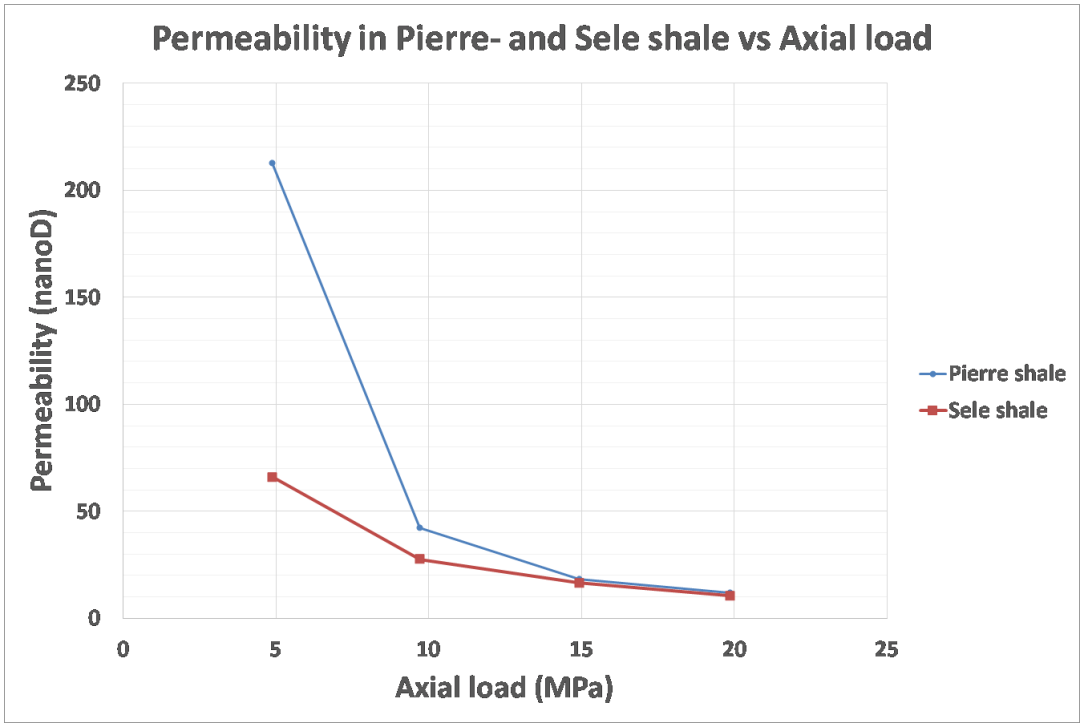

Figure 6.3: *Permeability in Sele and Pierre shale*

The Sele sample showed very similar behaviour, but with a much lower permeability under 3 MPa axial load.

Both the Pierre and Sele samples were calculated to have very low final permeabilities, at 18 MPa axial load, of 12 nD and 11 nD, respectively.

6.1.2 Porosity and clay content

An interesting property is also the porosity development in the samples. A drop in the porosity values is clear in the kaolinite samples. In the smectite samples, it is believed that more datapoints would have been beneficial to tell if the same behaviour would have been observed. More in the following sections.

6.1.2.1 Quartz-Kaolinite

Porosity in most of the kaolinite samples were found in 2017 by Oftedal. This year, an "extension" of 10% and 20% samples was added. As seen in Figure 6.4, there is a clear tendency of a "bottom point" at 50% clay content - a further discussion as to why this happens is included in section 6.2, but to understand what happens one have to consider the grain distribution geometry at the micro-scale.

Mondol (2009) also made porosity measurements in his quartz-kaolinite experiments, although with a different porosity bottom point. His results are rendered in Figure 6.5.

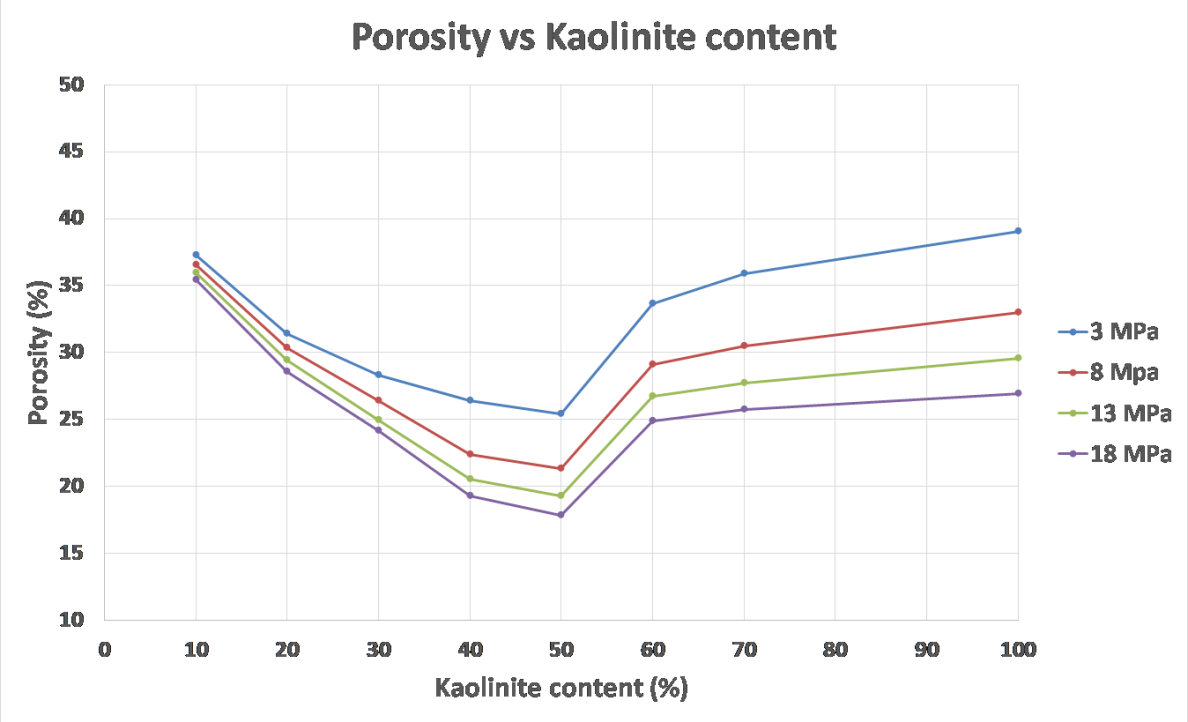

Figure 6.4: *Porosity vs kaolinite content*

It should be noted that the porosity values for the 70%-kaolinite sample by Oftedal (2017) have been adjusted for a new initial pore volume. The reason is quite simply that the values from Oftedal (2017) had a systematic and somewhat irrational drop in porosity for this clay ratio. This was not investigated further at the time, but it turns out that the input values in the porosity calculation from the LVDT's contained a discrepancy. This has now been corrected, and Figure 6.4 displays the corrected (and more rational) values.

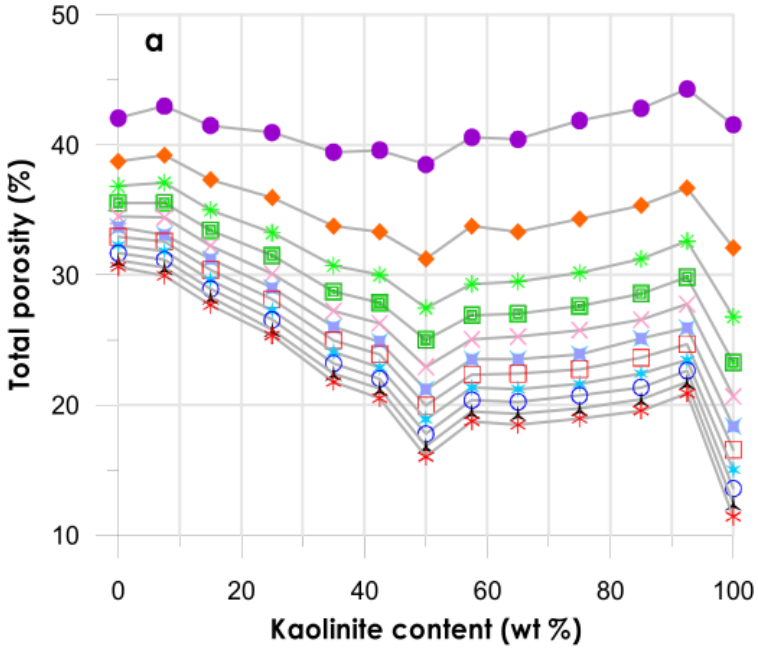

Figure 6.5: *Porosity vs kaolinite content (Mondol, 2009, p. 2142)*

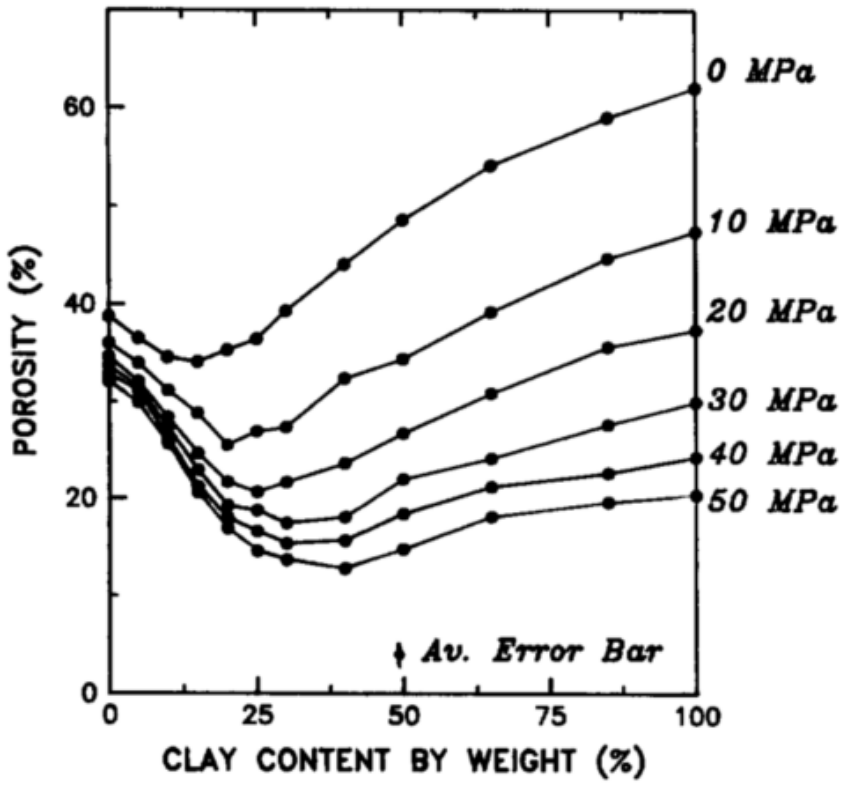

Figure 6.6: *Porosity vs kaolinite content (Han et al., 1992, p. 556)*

Mondol's (2009) results for a 100%-clay sample do not correlate with results from the current project. However, the results from Han et al. (1992) shown in Figure 6.6 do

correlate with the current project trend-wise, but with some discrepancy regarding the numerical values.

There is a trend showing in Figure 6.6 suggesting that the porosity low point is obtained at larger axial loads as the clay content is increased. In the work of Han et al. (1992), approximately the same quartz grain size as in this project was used (280 +/- 60μm) - although larger than Mondol (2009).

6.1.2.2 Quartz-Smectite

The porosity in the quartz smectite samples showed an increasing trend from the 40% clay sample. Due to a limited time-frame, further tests on smectite samples were not conducted - tests on smectite samples proved to be much more time consuming than the kaolinite samples, consolidation time was normally 2-3 times. More tests on samples with smectite content lower than 40% would have given information on the porosity development in the samples containing less than 40% and might help to determine an even better trend. Figure 6.7 displays the results.

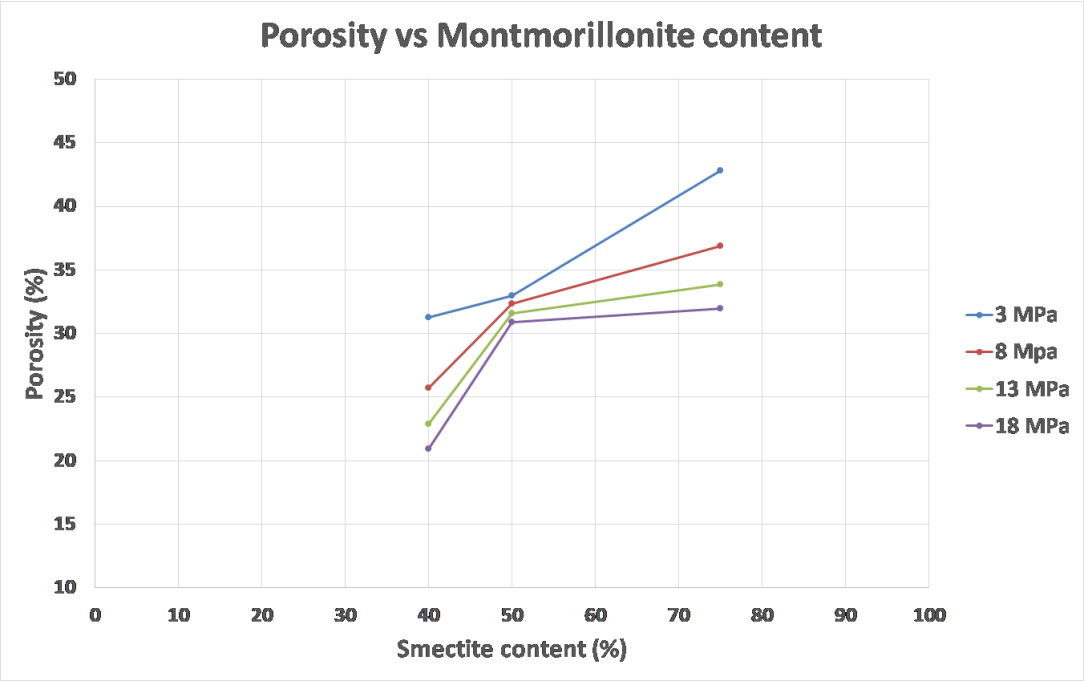

Figure 6.7: *Porosity vs smectite content*

Quite notable is the large spread in porosity in the 40% and 75% clay samples compared

to the 50% sample. Possibly due to packing effects where the 50/50 ratio clearly causes little variation in porosity compared to the other two. The same effect is observed in the 30% kaolinite sample from considering Figure 6.8. Here, the 50% smectite and 30% kaolinite samples are seen as the lines with a much lower gradient than in the other samples (closer to horizontal) - indicating that packing effects at these ratios cause the pore volume to be occupied already at relatively low compaction loads.

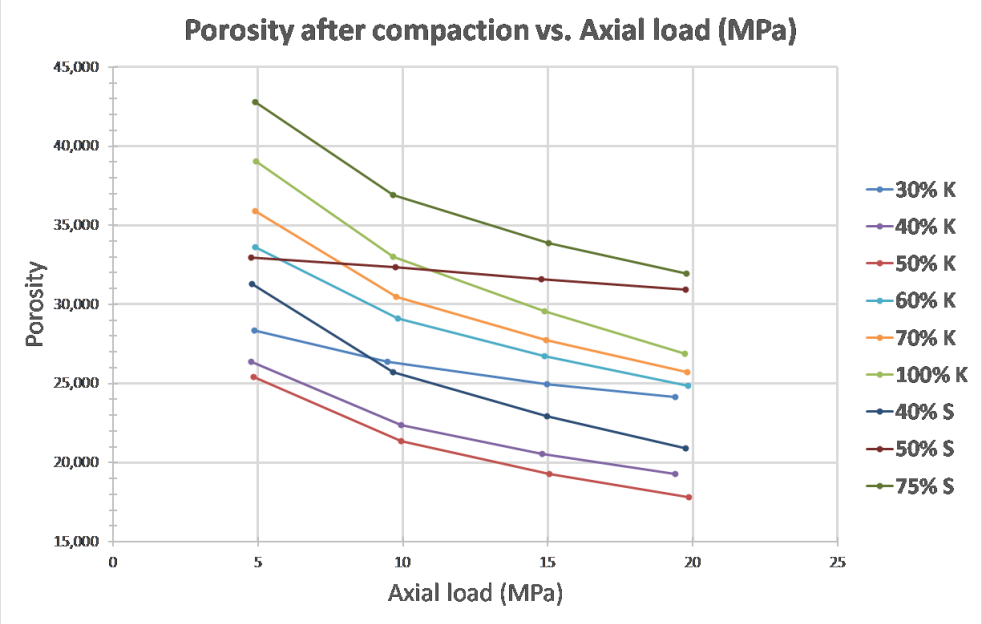

Figure 6.8: *Porosity development in kaolinite and smectite samples*

6.1.3 Ultrasonic data

Ultrasonic measurements were acquired from all the experiments performed in 2018. P-wave velocity was obtained and considered - telling us something about the degree of compaction in the sample and how the changing matrix affected the P-wave velocity. After the wave velocity was determined, the acoustic impedance was calculated - an important factor in the determination of annulus material from wireline acoustic logs. Quite obvious is the difference in travel time between the 10% kaolinite sample, 40% smectite sample and Pierre shale compared to the other samples. In the 10% kaolinite sample, the quartz is thought so abundant that it constitutes the load bearing matrix, thus having an impact on the travel time where the first arrival is recorded through the

quartz grains. In the same sample, there is an unexpected drop in wave velocity for

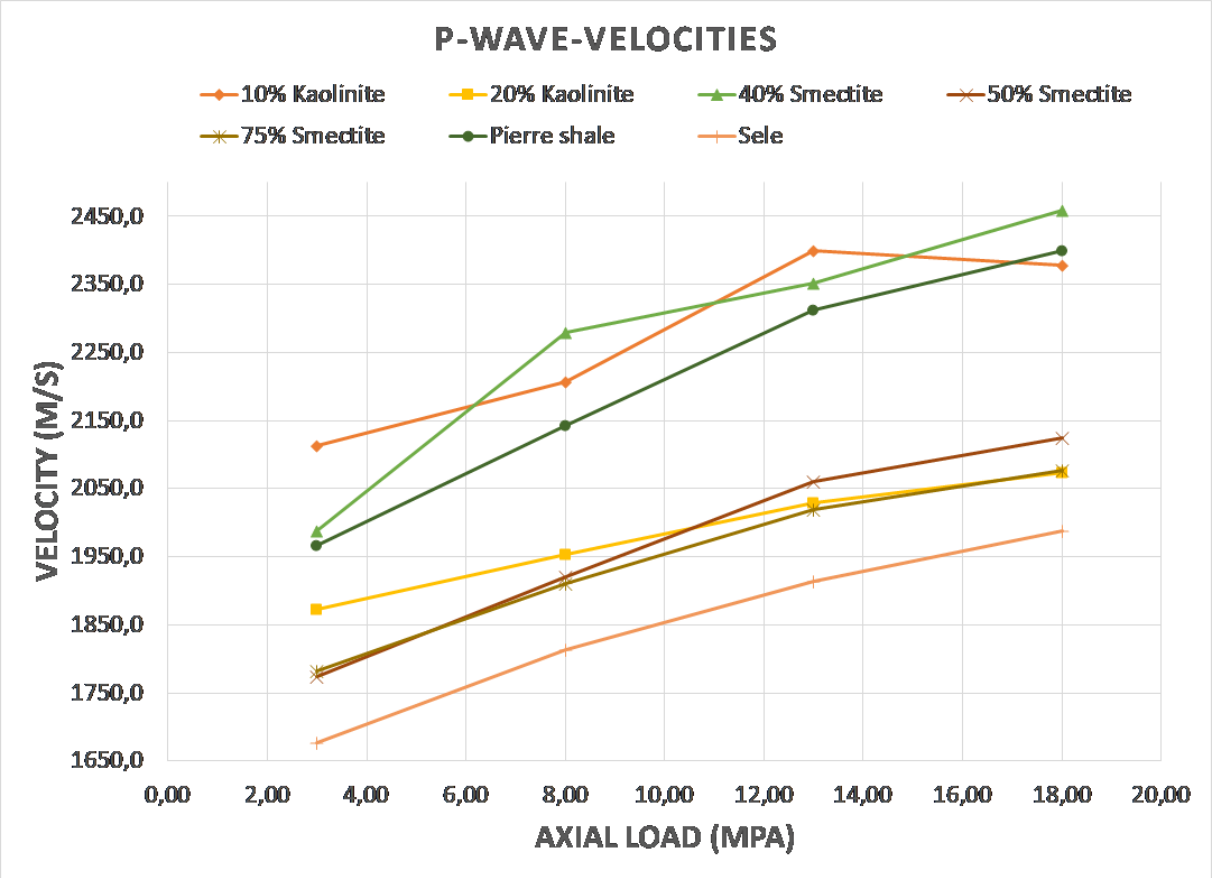

Figure 6.9: *P-wave velocity in all samples*

the 18 MPa effective stress case - the reason for this is unclear, possibly due to some inaccuracies in the ultrasonic equipment.

The results in Figure 6.9 were used to calculate the acoustic impedance in the samples, which is displayed in Figure 6.10. For comparison purposes, $Z_{water} = 1.48 * 10^6$ with a P-wave velocity in water of about 1450 m/s.

Evidently from Figure 6.9, there are three datasets that are distinct regarding the P-wave-velocity, the 10% kaolinite sample, the 40% smectite sample and the Pierre sample. In the sample with 90% quartz content, this is not very surprising due to the quartz constituting a stiff framework. However, from the acoustic impedance analysis, the difference in density in the 10% kaolinite sample is clear as the impedance is considerably lower than in the Pierre and the 50% smectite sample.

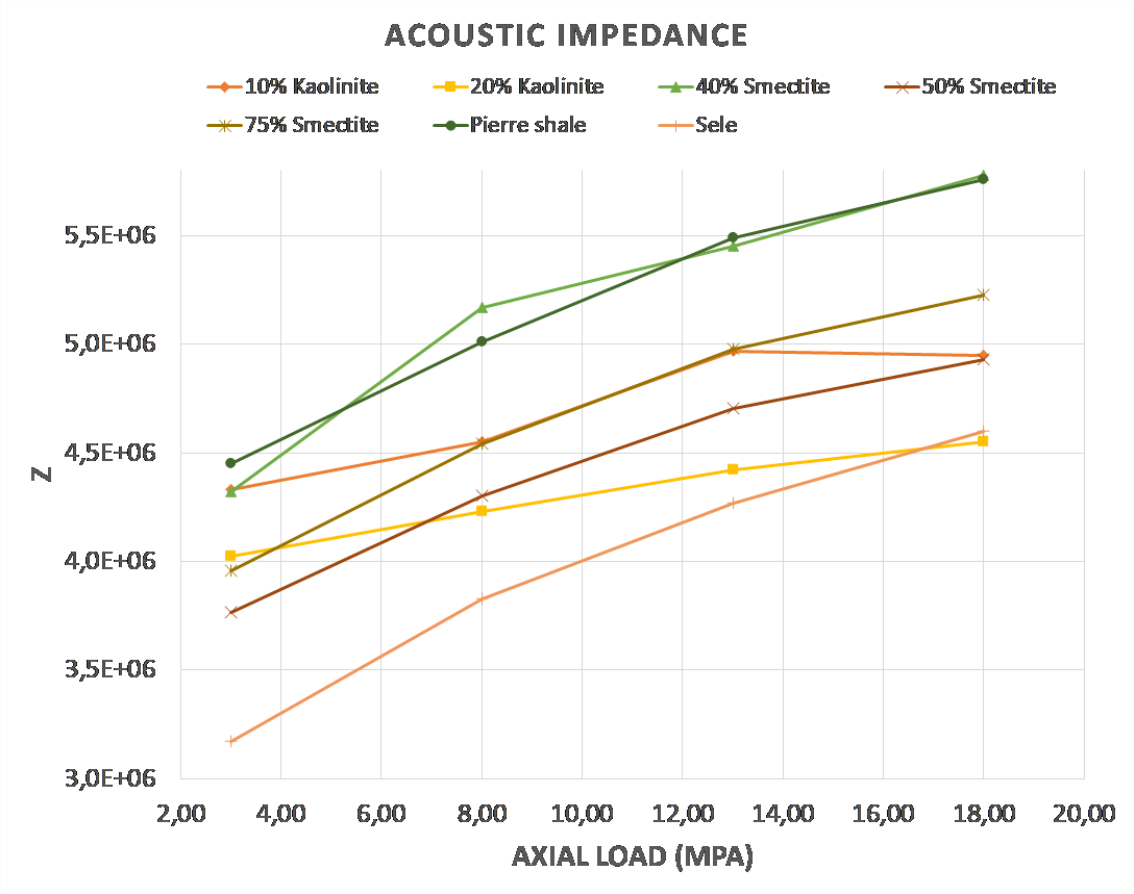

Figure 6.10: *Acoustic impedances*

6.2 Discussion

In this section, the most relevant results will be discussed. An attempt to identify reasons for the most clear trends will be made

6.2.1 Permeability results

The results from the permeability analysis showed a clear indication that particle size plays a significant role in how tight properties the samples exhibited. The quartz-kaolinite samples' lowest permeability was in the 100% kaolinite case with 161 nD at 18 MPa effective axial stress. In general, the permeability in the kaolinite samples were in the micro-Darcy range whereas the quartz-smectite samples, Pierre shale and Sele shale all were in the nano-Darcy range. It is thus clear what the packing effects of smaller lay

particles in the samples cause with regards to the rock tightness, Pierre and Sele both have a portion of clay minerals smaller than kaolinite. Regarding the smectite, we already know that the difference in particle size in considerable compared to kaolinite and it was therefore expected beforehand that an effect on the tightness would be observed.

Regarding the use of such materials in a real scenario, the materials have a lower permeability than what is considered as normal in a set Portland cement: 20 μD (Kristiansen, 2015). Important to note is that the self-made mixtures can be considered as somewhat "extreme" cases. One will not find a material with only those two constituents. However, by considering the permeability results and correlating with results from the ultrasonic measurements, one can obtain an impression of what type of material has good sealing capabilities based on wireline logs.

Especially interesting is the Sele shale. The acoustic impedance results (Figure 6.10 in that material were considerably low compared to the other datasets, but still the permeabilities measured were among the lowest in any of the samples (11 nD). This indicates that one cannot conclude on sealing capability based on density alone - one also has to consider the packing in the material.

6.2.2 Porosity results

The porosity development in the samples was quite as expected. In general, it was expected to see a tendency of higher porosity when the clay content increased. For the smectite samples, this held true in all the tests. Due to the lack of experimental data for smectite samples (<40% clay content was not investigated), it is not possible to identify a clear trend in ratios lower than this - something that could possibly be included in future studies of similar nature.

In the kaolinite samples, the data points are more and we are able to draw more conclusions on what happens as the ratio changes. Quite notable is the apparent drop in porosity at 50% clay content. To try and understand that behaviour, one must take a closer look at what happens at the microgeometrical scale. Han et al. (1992, p. 557) presented Figure 6.11 that displays an essential factor in the process of understanding

the porosity "low point" value. In Figure 6.11, c denotes the concentration of clay and ϕ_s

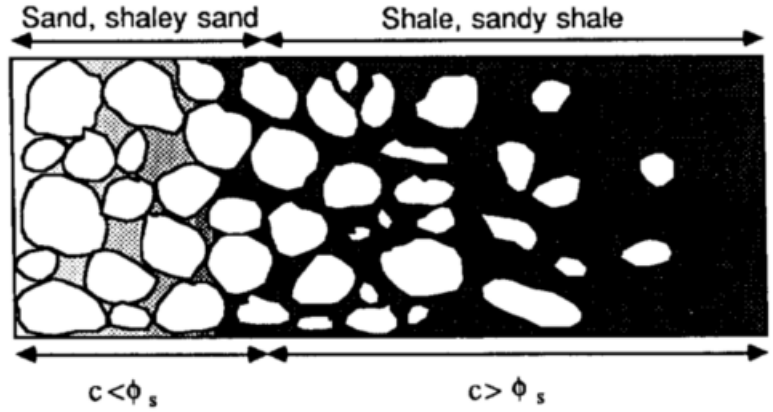

Figure 6.11: *Shaly sand/sandy shale (Han et al., 1992, p. 557)*

denotes the porosity considering the sand grains alone. In our own discussion, we separate between the concentration of kaolinite ($c_{kaolinite}$) and smectite ($c_{smectite}$). In general, if one considers a sample with $c = 1.0$, the situation is described in the right side of Figure 6.11. As one moves to the left on the "axis", c decreases and the sand grains take up a larger and larger part of the volume before they eventually become "dominant" and constitute the load-bearing matrix in the sample. The transition between "sandy shale" and "shaly sand" occurs when $c = \phi_s$. Further to the left, less and less clay is dispersed in the sand pore space and the porosity thus increases as the clay content decreases. This is possible because of the significant difference in particle size between the quartz grains and the clay particles.

Figure 6.7 clearly displays that this effect does not take place when $0.4 < c_{smectite} < 0.75$, as far as our data points go, it is clear that porosity drops further as $c_{smectite}$ goes below 50%.

For comparison purposes, it should be noted that in the experiments by Mondol (2009), silt with grain size 4-40μm was applied whereas much larger grain size has been used in this project.

Han et al. (1992) conducted experiments on Ottawa sand and pure kaolinite, shown in Figure 6.6, in which they found that there was a drop in porosity in samples containing 20-40% clay. In that work, larger sand grains that from Mondol (2009) was applied. Therefore it is interesting to consider those results as well.

6.2.3 Discussion on methodology

The methodology has been described in a separate section. A few possible areas of improvement will be briefly mentioned here.

6.2.3.1 Sample preparation

In the experiments, one of the most apparent possible sources for error was the mixing of the dry synthetic materials when making the samples. When weighing up the material, it was done to an accuracy of +/- 0.05 grams. Making sure that all material was included in the sample was easily done with the quartz as the grains are quite large. It was more challenging with the clay due to the very small particles that are easily air-born when stirred - especially when mixing the smectite where the particles are considerably smaller than in the kaolinite.

The amount of clay material that potentially got lost when making the samples was very little. However, it is worth to explore a new way of doing the procedure if this provides a more controlled way of doing it.

For future studies in which mixing of synthetic materials will be essential, inspiration might be taken from Han et al. (1992). In stead of gradually mixing dry material with water, all the dry material was mixed together in a sealed container until the mixture between sand and clay appeared homogeneous by visually inspecting the material. The sample was then put in a container and exposed to a vacuum before pore fluid was injected at one end of the sample. By doing that, the under-pressurized container sucked in the fluid and saturated the dry material with the fluid. For further description, the reader is directed to read the work of Han et al. from 1992.

6.2.3.2 Assumptions in mathematical model

In Chapter 5, the procedure for calculating the transient permeability with equations from a model presented by Reuschle (2011) was introduced - a model originally presented by Brace et al. (1968). That model includes an assumption regarding the storage volume

in the sample (C_s) compared to the pore fluid volume in the pore fluid circuits above and below the sample. That assumption allows for an exponential approximation of the pressure pulse decay. However, that is an assumption that not necessarily holds true in the experiments in this project. In a case where C_s is not negligible, a more complex equation derived by Hsieh et al. was derived by Bredehoeft et al. (1981).

Bredehoeft et al. (1981) showed in their work that there is an effect on the pressure pulse-decay curves when the storage volume in the sample is non-negligible. However, the model presented in that work is problematic due to its complexity which makes it difficult to use in a practical situation like in this project. According to Reuschle, one simple way to decide whether or not Brace et al. (1968) "simplified" version is valid or not is to plot the differential pore pressure decay vs. time in a semi-log plot and check its linearity. If a linear curve is obtained, there is no apparent reason to change the approach - leaving the approximation by Brace et al. (1968) unaltered.

This "linearity-criterion" has been investigated to hold true for all samples in this project. Figure 5.5 is a good example of a pressure decay curve obtained in this project. In that figure, the linearity in the semi-log plot is clear, thus convincing further that the approach of our choice is good.

In 2017, Oftedal made a remark in his report that for the following tests that would take place in 2018, the upstream/downstream circuit volumes should be increased so that the assumption presented by Brace et al. (1968) would be supported further. However, after consultation with the author of Reuschle (2011), it was decided not to alter the circuit volumes. The most notable argument for that decision is that too large circuit volumes could have made it problematic to obtain a pressure differential over the sample that was large enough, especially considering the equipment at hand, in which two small needle valves were all that could be used to create a volumetrically-induced pressure pulse in the system.

Moreover, if one were to substantially increase the circuit volumes, the pressure pulse would in practice have to be increased accordingly - causing a much more time-consuming test which is not only more impractical, but also presents other challenges like a higher

chance of worsened data quality due to temperature fluctuations in the surroundings.

6.3 Challenges

Some challenges presented themselves in the laboratory experiments of the project. One of the most obvious ones is related to the moment arm. Because the moment arm is hinged and moves downward as a sample inside the cylinder compacts, the axial load will vary during the compaction phase of a sample as a result of the varying horizontal distance from deadweight to the contact point between piston and vertical gravity force from the deadweight. However, this was not a very serious issue as the trend in the samples is just as important as the numerical values themselves. Therefore, it is encouraged to continue using the same equipment for similar studies in the future - with the knowledge of the challenges that can come with it. To better control the load that is applied to the sample, weights with smaller mass than the current ones could be manufactured quite easily and would help when only small increments in the load are needed.

The mixing of the synthetic samples were done in a very controlled manner. But, by taking inspiration from the work of Han et al. (1992), the mass control while mixing the dry material could be even better. Especially when mixing smectite, with its extremely small particles, the method presented by Han et al. (1992) could be beneficial.

7 Conclusion

In the beginning of the project (and of this report), the main objectives were established that would to a large extent shape the work of the project. Permeability measurements have been successfully performed in a series of experimental tests on samples containing different materials (see Table 3 for all materials).

A clear tendency of very low permeability was observed in the smectite samples and in the Pierre shale and Sele shale with the lowest measured permeability of 5 nD in the 75% smectite sample, 11 nD in the Sele shale and 12 nD in the Pierre shale. All after being compacted by 18 MPa axial stress. Some of the kaolinite samples also had low permeabilities, especially in the samples with higher clay content than 30%, but none lower than 161 nD.

In addition to the permeability measurements, ultrasonic data were acquired and it was observed that although with low density and a propagating P-wave-velocity not much higher than in that of water, a material can still be low-permeable. A perfect example is the Sele shale, where the acoustic impedance was low, but still the sample was very tight.

One might ask how this project is relevant to the industry - why has the project been incorporated in SINTEF's P&A project? The answer to that question appears quite apparent when considering the importance of widening the scope of knowledge on such a matter as this. It has been deemed interesting to see how synthetic clay samples and real material from the field behaves during the test regime that has been conducted in this study. Not only are permeability and porosity important parameters, but also acoustic impedance - providing more information on a possible annular material and its properties.

If one encounters formation intervals in real life in which the mineralogy is known and stress regime is modelled, the results from this project can help in knowing what kind of properties a rock with a similar structure could exhibit.

7.1 Suggestions for future work

During the course of this project, several points have been identified as possible interesting fields of study for future theses and/or publications.

- The ability of a trapped annulus volume to withstand an inwards moving plastic formation. Does a nearly incompressible annulus fluid have the ability to hole the formation back, or is it likely to escape through some line, valve or into formation?
- Simulation of situations in a plugged well where unforeseen circumstances lead to a pressure differential across a verified plug. Is that a scenario in which results from the current project can be applied?
- While tripping in/out of a well, surge and swab pressures are created that might induce an inwards/outwards flow through the wellbore. With similar mineralogy, results from this study might be used as parameters in a study of such effects.

Possible subjects for future studies are several, and within the scope of applying shale as a barrier material, there is still much left to do before a possible scenario where shale barriers are actively induced by the operator.

8 References

Asef, M.R., Farrokhrouz, M. 2013. *Shale Engineering: Mechanics and Mechanisms*. London: CRC Press/Balkema.

Batzle, M., Wang, Z. 1992. 'Seismic properties of pore fluids'. *Geophysics*, 57 (11), pp. 1396-1408.

Baptist O.C., Land C.S. (1965) 'Effect of Hydration of Montmorillonite on the Permeability to Gas of Water-Sensitive Reservoir Rocks. *Journal of Petroleum Technology*, 17 (10), pp. 1213-1218.

Boerngen, J.G., Gill, J.R, Schultz, L.G., Tourtelot, H.A. 1980. 'Composition and properties of the Pierre Shale and equivalent rocks, northern Great Plains region'. Available at: `https://pubs.usgs.gov/pp/1064b/report.pdf` [Accessed 30 May 2018].

Brace, W.F., Frangos, W.T., Walsh, J.B. 1968. 'Permeability of granite under high pressure'. *Journal of Geophysical Resarch*, 73(6), pp. 2225-2236.

Bredehoeft, J.D., Hsieh, P.A., Neuzil, C.E., Silliman, S.E., Tracy, J.V. 1981. *A transient laboratory method for determining the hydraulic properties of "tight" rocks—I. Theory.* Int. J. Rock. Mech. Min. Sci. Geomech. Abstr., 18(3):245–252. doi:10.1016/0148-9062(81)90979-7

Bruce, S., Cook, J., Meehan, R., Swan, G. 1989. 'Strain Rate Effects in Kimmeridge Bay Shale'. *International Journal of Rock Mechanics and Mining Sciences & Geomechanics Abstracts*, 26(2), pp. 135-149.

Callister, Jr, W. D., Rethwisch, D. G. 2014. *Materials Science and Engineering - An Introduction*. 9th ed. New York: John Wiley & Sons.

Carlson M.R. 2003. *Practical Reservoir Simulation: Using, Assessing, and Developing Results*. Tulsa: PennWell Books.

Çengel Y. A., Cimbala J.M. 2014. *Fluid Mechanics: Fundamentals and Applications*. 3rd ed. Singapore: McGraw-Hill Education.

Cosenza, P., Goncalves, J., Marsily, G. De, Rousseau-Gueutin, P., Violette, S. 2010. 'What is the significance of pore pressure in a saturated shale layer?' *Water Resources Research* 46(4). doi:10.1029/2009WR008090

Encyclopaedia Britannia. (No date). Available at: `https://www.britannica.com/science/clay-mineral/images-videos` [Accessed 5 June 2018].

Fjær, E., Holt, R.M., Horsrud, P., Raaen, A.M., Risnes, R. 2008. *Petroleum Related Rock Mechanics*. 2nd ed. Amsterdam: Elsevier.

Han, D., Marion, D., Nur, A., Yin, H. 1992. 'Compressional velocity and porosity in sand-clay mixtures'. *Society of Exploration Geophysicists*, 57(4), pp. 554-563.

Juma, N.G. 1998. 'The Pedosphere and Its Dynamics: A Systems Approach to Soil Science'. Vol. 1. Edmonton: Quality Color Press Incorperation. Available at: `http://www.soils.rr.ualberta.ca/pedosphere/content/section06/page03.cfm`

Kristiansen, T.G. 'Why Shale Could be Used as a Permanent Well Barrier Element' [Powerpoint presentation]. *Plug & Abandonment Seminar 2015 - Stavanger*. Available at: `https://www.norskoljeoggass.no/globalassets/dokumenter/drift/presentasjonerarrangementer/plug--abandonment-seminar-2015/10---shale-as-well-barrier-material_bp_tgk-final.pdf` [Accessed 5 May 2018].

Lal, M. 1999. 'Shale Stability: Drilling Fluid Interaction and Shale Strength', *SPE Latin American and Caribbean Petroleum Engineering Conference*. Caracas, Venezuela, 21-23 April 1999. Society of Petroleum Engineers.

Li B., Wong R. 2013. 'Effect of Thermally Induced Deformation of Shale on Wellbore and Caprock Integrity', *SPE Heavy Oil Conference Canada*. Calgary, Alberta, Canada, 11-13 June 2013. Society of Petroleum Engineers.

Matthews, C.S., Russell, D.G. 1967, *Pressure Buildup and Flow Tests in Wells*. New York: Henry L. Doherty Memorial Fund of AIME.

Miska, S.Z., Mitchell, R.F. 2011. *Fundamentals of Drilling Engineering*. Vol. 12. Society of Petroleum Engineers

Mondol, N.H. 2009. 'Porosity and permeability development in mechanically compacted silt-kaolinite mixtures'. SEG international exposition annual meeting. Houston: USA. pp. 2139-2143.

Norwegian Oil and Gas Association and The Federation of Norwegian Industries (NORSOK D-010). 2013. *Well integrity in drilling and well operations.* Lysaker: Standards Norway. Available at: `http://www.npd.no/Global/Norsk/5-Regelverk/Skjema/Bronnregistrering/NORSOK-D-010-2013-Well-integrity-and%20Well-operations-rev%204.pdf` [Accessed 5 May 2018].

Oftedal, I.W. 2017. 'Transient Permeability Measurements in consolidated sand-clay samples'. *Not published. Submitted to The Norwegian University of Science and Technology 19th of December, 2017 - not available online.*

Oort, E.V. 2013. 'On the physical and chemical stability of shales'. *Journal of Petroleum Science and Engineering*, 38(3), pp. 213-235.

Reuschle, T. (2011), Data report: *Permeability measurements under confining pressure, expeditions 315 and 316, Nankai Trough.* Proc. Integr. Ocean Drill. Program, 314/315/316, 17 pp., doi:10.2204/iodp.proc.314315316.205.2011.

Appendices

A Apparature

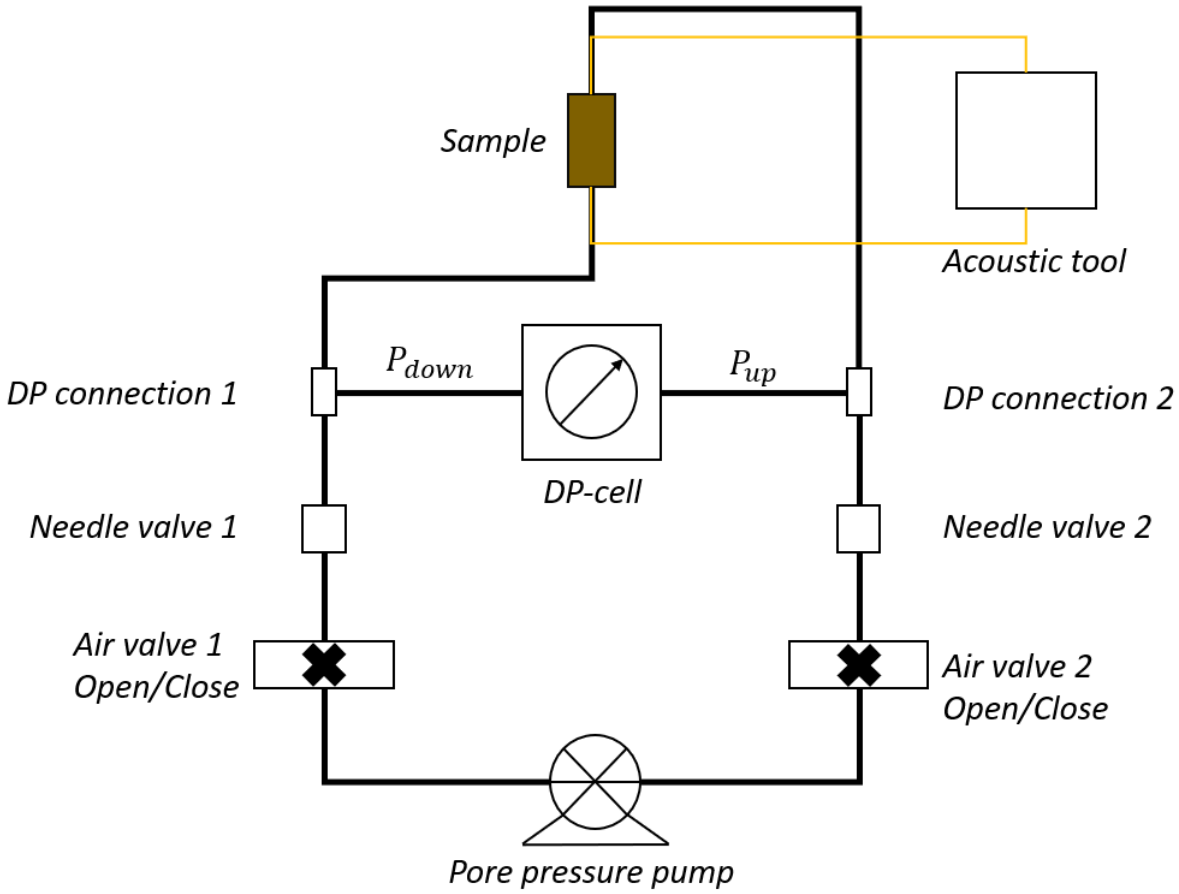

Figure A.1: *Schematic of the test apparature*

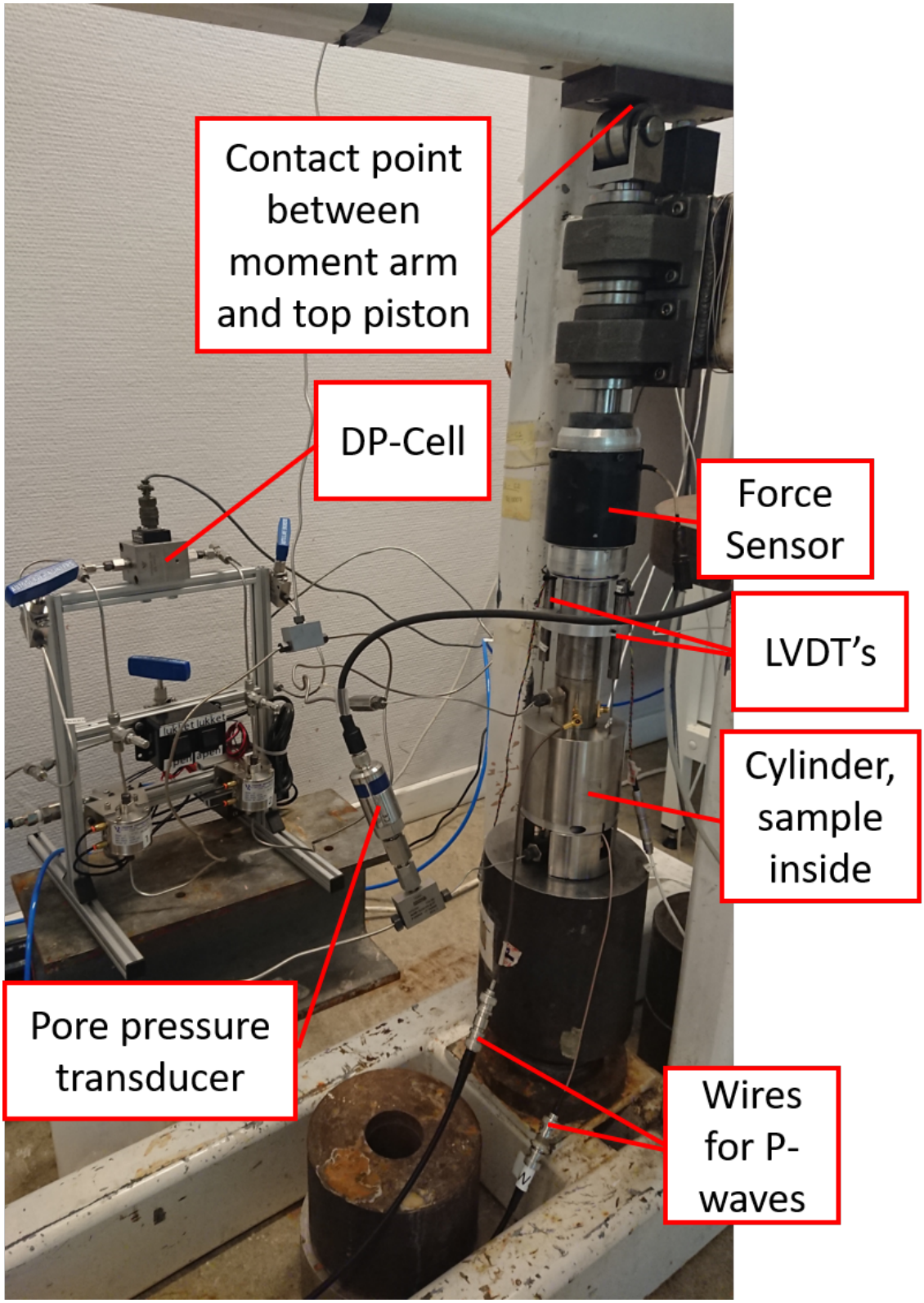

Figure A.2: *Physical equipment under moment arm*

Figure A.3: *Pore pressure pump, the two cylinders with a piston each are seen*

Figure A.4: *Computer with data-logging on right and compressional wave velocity measuring on the left*

Figure A.5: *Deadweight hung off from moment arm*

B Test results in synthetic samples

	Material ratios			Properties			
Effective stress (Mpa)	Quartz	Kaolinite	Smectite	Porosity (%)	Permeability (nD)	Travel time (ms/m)	Impedance (Pa s/m3)
3	0	1	0	39,06	538,87	na	na
3	0,3	0,7	0	35,89	988,43	na	na
3	0,4	0,6	0	33,63	1088,12	na	na
3	0,5	0,5	0	25,42	1137,80	na	na
3	0,6	0,4	0	26,36	843,84	na	na
3	0,7	0,3	0	28,33	2552,22	na	na
3	0,8	0,2	0	31,41	2676,27	1,17011E-05	4022362,282
3	0,9	0,1	0	37,27	5205,20	1,17118E-05	4331070,003
3	0,25	0	0,75	42,80	21,86	5,99862E-06	3958995,248
3	0,5	0	0,5	32,97	26,43	7,38088E-06	3767803,193
3	0,6	0	0,4	31,29	33,98	7,57991E-06	4322431,723

Figure B.1: *Results in synthetic samples - 3 MPa axial load*

	Material ratios			Properties			
Effective stress (Mpa)	Quartz	Kaolinite	Smectite	Porosity (%)	Permeability (nD)	Travel time (ms/m)	Impedance (Pa s/m3)
8	0	1	0	33,00	320,22	na	na
8	0,3	0,7	0	30,50	538,33	na	na
8	0,4	0,6	0	29,09	567,85	na	na
8	0,5	0,5	0	21,35	667,26	na	na
8	0,6	0,4	0	22,39	587,29	na	na
8	0,7	0,3	0	26,39	2081,35	na	na
8	0,8	0,2	0	30,35	2387,46	1,10521E-05	4228329,483
8	0,9	0,1	0	36,56	4200,52	1,10888E-05	4549353,049
8	0,25	0	0,75	36,91	8,51	5,07693E-06	4543492,08
8	0,5	0	0,5	32,33	12,81	6,17929E-06	4300805,877
8	0,6	0	0,4	25,70	13,92	6,41399E-06	5171516,452

Figure B.2: *Results in synthetic samples - 8 MPa axial load*

	Material ratios			Properties			
Effective stress (Mpa)	Quartz	Kaolinite	Smectite	Porosity (%)	Permeability (nD)	Travel time (ms/m)	Impedance (Pa s/m3)
13	0	1	0	29,55	231	na	na
13	0,3	0,7	0	27,72	313	na	na
13	0,4	0,6	0	26,73	340	na	na
13	0,5	0,5	0	19,27	369	na	na
13	0,6	0,4	0	20,53	319	na	na
13	0,7	0,3	0	24,97	1598	na	na
13	0,8	0,2	0	29,45	2175	1,0502E-05	4423919,375
13	0,9	0,1	0	35,95	3714	1,0102E-05	4970556,215
13	0,25	0	0,75	33,85	6	4,5786E-06	4977348,75
13	0,5	0	0,5	31,60	8	5,5605E-06	4706036,525
13	0,6	0	0,4	22,91	10	5,7718E-06	5450131,838

Figure B.3: *Results in synthetic samples - 13 MPa axial load*

	Material ratios			Properties			
Effective stress (Mpa)	Quartz	Kaolinite	Smectite	Porosity (%)	Permeability (nD)	Travel time (ms/m)	Impedance (Pa s/m3)
18	0	1	0	26,90	161	na	na
18	0,3	0,7	0	25,73	274	na	na
18	0,4	0,6	0	24,86	289	na	na
18	0,5	0,5	0	17,80	315	na	na
18	0,6	0,4	0	19,28	278	na	na
18	0,7	0,3	0	24,14	1321	na	na
18	0,8	0,2	0	28,57	1979	1,015E-05	4551581,145
18	0,9	0,1	0	35,42	2612	1,0107E-05	4948673,55
18	0,25	0	0,75	31,96	5	4,3296E-06	5229038,075
18	0,5	0	0,5	30,91	6	5,2421E-06	4931722,021
18	0,6	0	0,4	20,93	7	5,3974E-06	5779466,235

Figure B.4: *Results in synthetic samples - 18 MPa axial load*

C Other properties

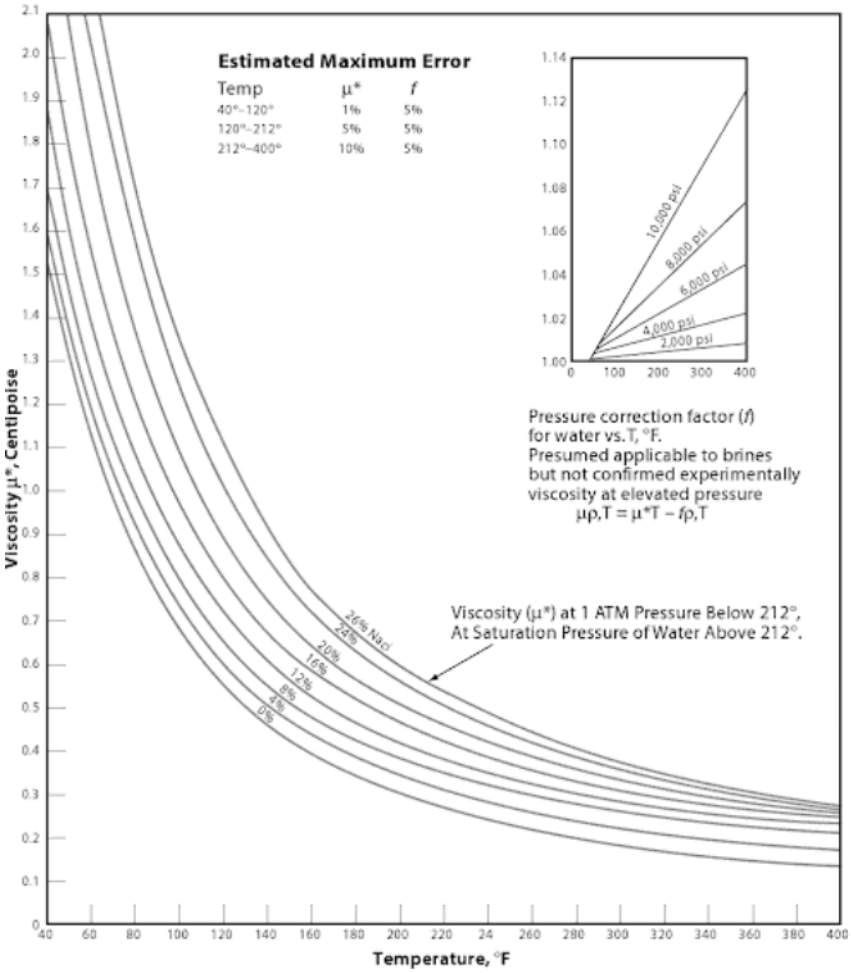

Figure C.1: *Common viscosity correlation in NaCl-brines (Matthews and Russell, 1967)*

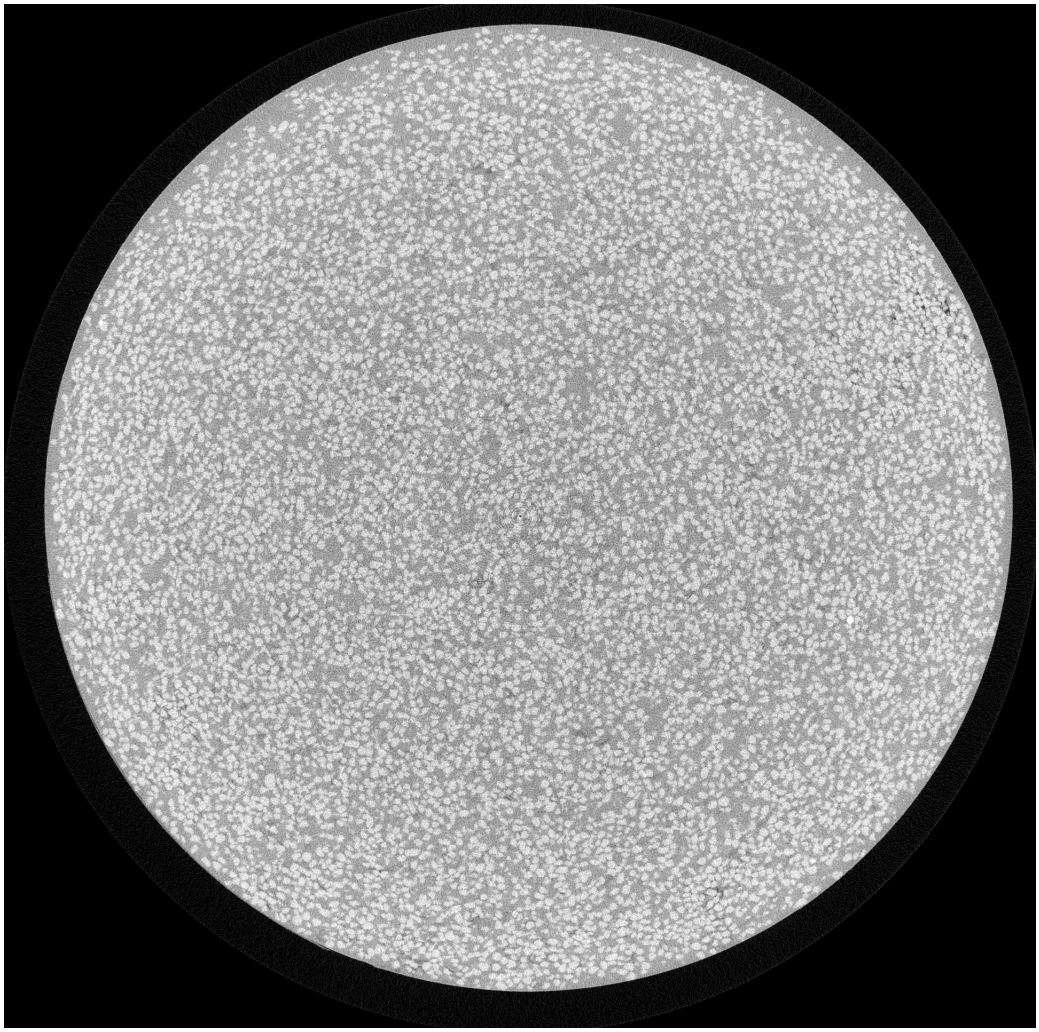

Figure C.2: *CT-scan of sample with 50% kaolinite, 50% quartz)*

In Figure C.2, there is a good display of the grain distribution within the sample, indicating that the mixing of the powdered materials was performed in a satisfactory manner.

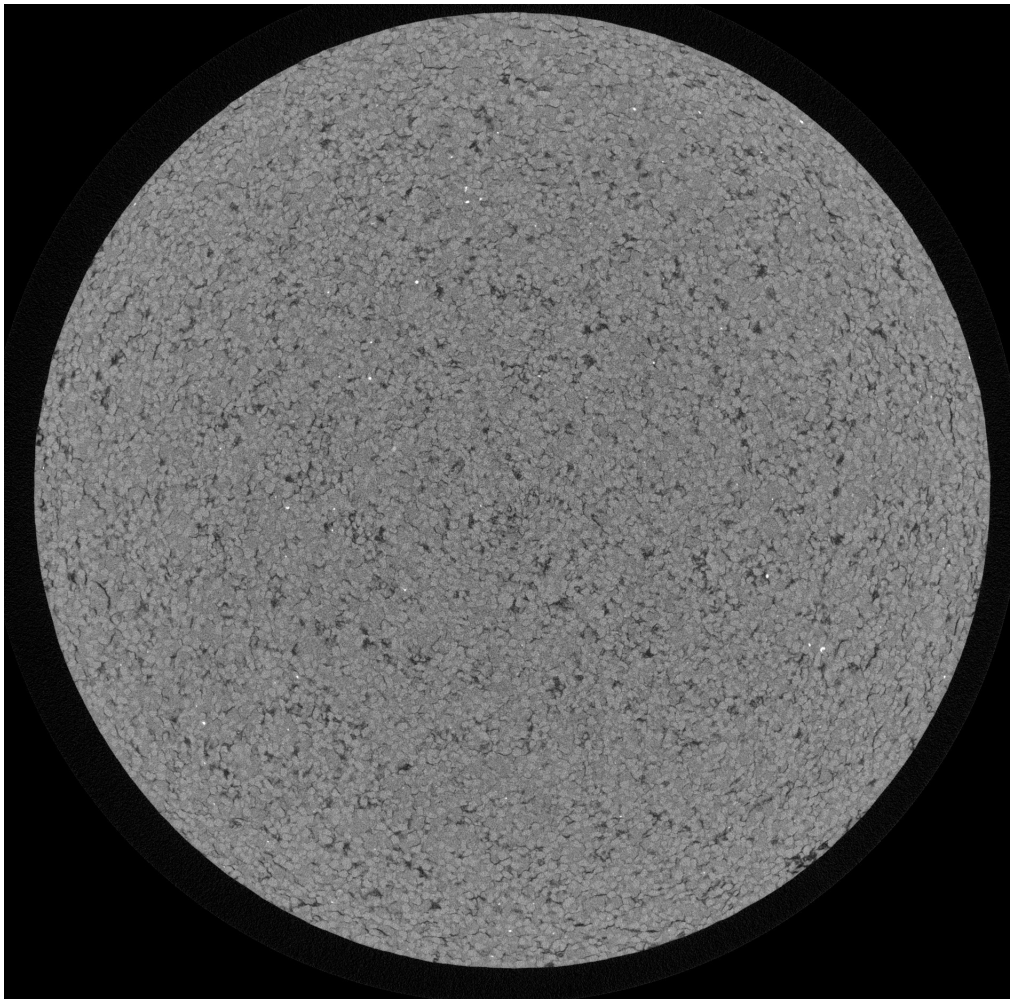

Figure C.3: *CT-scan of sample with 50% smectite, 50% quartz)*

Although with the same quartz-clay ratio as in Figure C.2, the apperance in the ct-scan of the 50% smectite, 50% quartz sample in Figure C.3 is quite different. It is not as easy making a distintion between the minerals, which might be explained by the much smaller clay particle size which allows more dense packing of the smectite.